Climatic conditions inside nuclear reactor containments

Evaluation of moisture condition in the concrete within reactor containments and interaction with the ambient compartments

OXFALL, Mikael

2016

Document Version:
Publisher's PDF, also known as Version of record

CLIMATIC CONDITIONS INSIDE NUCLEAR REACTOR CONTAINMENTS

Evaluation of moisture condition in the concrete within reactor containments and interaction with the ambient compartments

LUND UNIVERSITY

Mikael Oxfall

Doctoral thesis, Report TVBM-1035, Division of Building Materials,
Faculty of Engineering, Lund University, Lund 2016

Lund University, Faculty of Engineering, Division of Building Materials
P.O. Box 118
SE-221 00 Lund, Sweden
www.byggnadsmaterial.lth.se

ISRN LUTVDG/TVBM – 16/1035 – SE(1-81)
ISSN 0348-7911 TVBM
ISBN 978-91-7623-820-2 (Print)
ISBN 978-91-7623-821-9 (Pdf)
Printed in Sweden by Media-Tryck, Lund University
Lund 2016

Preface

This doctoral thesis is the result of research conducted since 2010 at the division of building materials at Lund University and at Vattenfall AB R&D-laboratories in Älvkarleby. The project has been financed by Energiforsk, the Swedish Electrical Utilities R&D Company, with constitutions from: Fortum, Karlstad Energi, Skellefteå kraft, Teollisuuden Voima, Uniper, Vattenfall and Swedish radiation safety authority. Their financial support is gratefully acknowledged.

I would like to thank my supervisors Prof. Lars Wadsö, Dr. Peter Johansson, Adj.prof. Manouchehr Hassanzadeh for all of their support and the encouragement during these last six years. I wold like to express my greatest gratitude to all personal at Forsmark and Ringhals that has been involved in this study and assisted me during my in situ work. I would like to thank the board members in the Energiforsk nuclear concrete program and especially those included in my reference group; Ulrik Brandin, Uniper; Henrik Bäckström, Forsmark KG; Johan Klasson and Johanna Spåls, Ringhals.

I would like to thank all my colleges both in Lund at the division of building materials and at the civil engineering group at Vattenfall AB in Älvkareby. A special acknowledgment is expressed to my college and friend Dr. Martin Rosenqvist for lots and lots of discussions and to Dr. Bojan Stojanovic for encouragement and advices.

I would like to thank my family and friends for all encouragement and love throughout this adventure. Finally I would like to express my deepest love and gratitude to Anna for all the love, patience and support and for listening to my disguised monologues.

List of appended papers

I. MOISTURE PROFILES IN CONCRETE WALLS OF A NUCLEAR REACTOR CONTAINMENT AFTER 30 YEARS OF OPERATION

M, Oxfall. P, Johansson. M, Hassanzadeh
Proceeding: Presented at the Nordic Concrete Research Symposium XXII, Reykjavik, Island, August 4–7 2014.
Nordic Concrete Research, Publication No. 50. Editor: D. Bager. 532 pp.

II. ASSESSMENT OF FACTORS THAT MAY AFFECT THE MOISTURE- AND TEMPERATURE VARIATION IN THE CONCRETE STRUCTURES INSIDE NUCLEAR REACTOR CONTAINMENTS

M, Oxfall. P, Johansson. M, Hassanzadeh
Proceeding: Presented at Fontevraud 8, Avignon, France, September 15-18 2014

III. MOISTURE LEVELS AND DRYING POTENTIAL OF THE CONCRETE IN SWEDISH REACTOR CONTAINMENTS

M, Oxfall. M, Hassanzadeh P, Johansson
EPJ Web of conferences, 2013. **56**, 03002

IV. LONG-TERM HYGROTHERMAL PERFORMANCE OF NUCLEAR REACTOR CONCRETE CONTAINMENTS – LABORATORY EVALUATION OF MEASUREMENT SETUP, IN SITU SAMPLING, AND MOISTURE FLUX CALCULATIONS

M, Oxfall. P, Johansson. M, Hassanzadeh
Cement and Concrete Composite, 2016. **65** 128–138

V. MOISTURE AND TEMPERATURE MEASUREMENTS IN POROUS MATERIALS UNDER NON-ISOTHERMAL CONDITIONS – EVALUATION AND ERROR LIMITATION

M, Oxfall. P, Johansson. M, Hassanzadeh (Manuscript)

VI. A MODEL TO PREDICT THE MOISTURE DISTRIBUTION OF THE CONCRETE STRUCTURES INSIDE NUCLEAR REACTOR CONTAINMENTS, AND ITS MOISTURE CONTRIBUTION TO THE ENVIRONMENTAL CONDITION

M, Oxfall. M, Hassanzadeh. P, Johansson. (Manuscript)

Contribution of co-authors

1. MO came up with the idea for the paper, planned the study, and collected and prepared the specimens with assistance from PJ. MO performed the measurements and analysis, and wrote the manuscript. MH and PJ contributed in planning the measurements and commented on the manuscript.
2. MO came up with the idea for the paper, planned the evaluation, collected and analysed the results and wrote the manuscript. MH and PJ commented on the manuscript.
3. MO came up with the idea for the paper, designed the measurement setup, conducted the measurements, analysed the results and wrote the manuscript. MH and PJ contributed in planning the study, assisted in each step, and commented on the manuscript
4. MO came up with the idea for the paper, designed the measurement setup, designed and assembled the experimental set-up, conducted the measurements, analysed the results and wrote the manuscript. MH and PJ contributed in planning the study, assisted in each step, and commented on the manuscript
5. MO came up with the idea for the paper, designed the measurement setup, produced the specimens, designed and assembled the experimental set-ups, conducted the measurements, designed and established the FEM models with theoretical assistance from Bojan Stojanovic and Magnus Åhs, analysed the results and wrote the manuscript. MH and PJ contributed in planning the study, assisted in each step, and commented on the manuscript.
6. MO came up with the idea for the paper, established the model, designed and wrote the MATLAB subroutines, planned and executed and analysed the measurements, analysed the results and wrote the manuscript. MH and PJ contributed in planning the study, assisted in each step, and commented on the manuscript.

Abstract

Safety is the top priority at a nuclear facility. The nuclear power plants are designed to prevent radioactive leakage to the surroundings, both during normal operation as well as in case of a severe accident. One of the most important structures in a nuclear power plant, with regard to safety, is thus the reactor containment wall. The containment wall is the last main barrier to prevent radioactive leakage, and it is designed to limit and control internal hazards if all other barriers fail. In order to understand and identify the potential deviation of the barrier, the effects of changes in the materials and how these changes occur and propagate have to be understood.

The work presented in this thesis concerns the moisture condition within nuclear reactor containment inner walls in addition to other concrete structures within the containments. The study aims to describe earlier, ongoing and future moisture contributions, and redistribution of moisture within and from the concrete structures within the containments.

An in situ measurement setup for long term monitoring of relative humidity and temperature in concrete was designed and installed in four reactor containments. The setup was used to monitor the actual conditions within the containments and in the concrete structures, and how they change over time. The measurements showed that all containments within the study complied with the regulated conditions with regard to temperature. The stable humidity in the air within the containments indicated that the dehumidification apparatus at the sites worked as anticipated, and that the measured conditions can be considered as "as-designed conditions", even though there is no regulation regarding permissible humidity. The results from the monitoring campaigns were further used to validate a model which was designed to describe the ongoing drying and moisture redistribution in the concrete structures.

The measurements and simulations done in this study show that the concrete structures within the reactor containment are still drying after approximately 30 years of operation, and will continue to dry and contribute with moisture to the ambient compartment for the remaining part of the service life for the reactors. The simulations presents that 35–45 % of the initial evaporable water had dried out, until this study, and that the amount for 60 years of operation is 45–55 %. The main drying has already occurred, and the moisture contribution to the ambient compartments will continue to decrease, thus contributing less moisture to the air in the containment in the future.

Keywords: Nuclear power plant, concrete, in site measurements, relative humidity, boiling water reactor, pressurized water reactor, mass transport.

Sammanfattning

Inom kärnkraftsindustrin är säkerhet den aspekt som prioriteras högst. Alla kärnkraftverk är designade för att i högsta möjliga mån förhindra läckage av radioaktivetet till omgivningen, både under drift och i händelse av en allvarlig olycka. Med anledning av detta är reaktorinneslutningens vägg en av de viktigaste säkerhetsrelaterade konstruktionerna vid en anläggning, detta då denna konstruktionsdel är den sista barriären för att förhindra ett läckage av radioaktiva partiklar. Reaktorinneslutningens vägg är designad för att begränsa och kontrollera effekten av inre olyckor om övriga barriärer fallerat. För att förstå och identifiera potentiella förändringar, samt effekter från åldring, av barriären behövs en ökad förståelse för hur ingående material ändras över tid.

Arbetet som presenteras i den här avhandlingen berör främst fuktförhållanden i reaktorinneslutningarnas väggar och till viss del övriga betongkomponenter lokaliserade i inneslutningarna. Studiens mål var att beskriva den tidigare, pågående, och framtida omfördelningen av fukt, både i betongkonstruktionerna samt fuktbidraget från betongen.

En mätuppställning för in situ långtidsmätning av relativ fuktighet och temperatur i betong designades och installerades för monitorering i fyra olika reaktorinneslutningar. Utrustningen användes för att mäta de aktuella förhållandena samt för att studera variationer över tid. Mätningarna gjordes både i inneslutningarnas betongkonstruktioner samt i omgivande luft. De utförda mätningarna visade att de temperaturer som uppmättes svarade mot de krav som ställts på konstruktionen. Vidare indikerade den stabila relativa fuktigheten i inneslutningarnas luft att anläggningarnas avfuktning fungerade väl och att det bör kunna antas att rådande nivåer överensstämmer med de avsedda fuktnivåerna. Resultaten erhållna från monitoreringen användes vidare för att validera en modell framarbetad för att beskriva den pågående uttorkningen och omfördelningen av fukt i inneslutningarnas betongkonstruktioner.

De samlade resultaten från simuleringarna och mätningarna i studien visar att uttorkning av reaktorinneslutningarnas betong fortfarande pågår efter runt 30 år i drift. Betongen kommer även i fortsättningen att bidra med fukt till inneslutningens utrymmen, enligt simuleringarna ända fram till dess att verken tas ur drift. Den sammanlagda uttorkningen fram till de utförda mätningarna motsvarar i storleksordningen 35–45 % av betongens initiala förångningsbara vatten. Motsvarande värde vid 60 års drift förutspås vara 45–55 %, huvuddelen av betongkonstruktionernas uttorkning har således redan inträffat och fukttillskottet till inneslutningens luft kommer att avta med tiden.

Nyckelord: Kärnkraftverk, betong, in situ mätningar, relativ fuktighet, kokvattenreaktorer, tryckvattenreaktorer, masstransport.

Abbreviations and Symbols

Abbreviations

AFt	Ettringite
AFm	Monosulphate
BWR	Boiling water reactor
CH	Calcium hydroxide
C-S-H	Calcium silicate hydrate
DSC	Differential scanning calorimetry
DTA	Differential thermal analysis
EPR	Evolutionary power reactor
ITZ	Interfacial transition zone
IAEA	International atomic energy agency
LOCA	Loss of cooling accident
LOI	Loss on ignition
LH-cement	Low heat-cement
NPP	Nuclear power plant
PWR	Pressurized water reactor
RUP	Reference unit power
RH	Relative humidity
TGA	Thermogravemetric analysis
VVER	Water–water energetic reactor
w/c-ratio	Water/cement-ratio

Symbols

c	Transport potential	[ ]
D_c	Diffusion coefficient	[ ]
$k(ø,T)$	Inverse slope of sorption isotherm	[m^3 kg^{-1}]
k_p	Effective permeability	[kg m^{-2}]
$K(ø)$	Hygrothermal coefficient	[K^{-1}]
M_w	Molar mass of water	[kg mol^{-1}]
p	Water vapour pressure	[Pa]
p_s	Water vapour pressure at saturation	[Pa]
P_{atm}	Atmospheric pressure	[Pa]
P_w	Pour water pressure	[Pa]
q_{liq}	Liquid flux	[kg m^{-2} s^{-1}]
q_{tot}	Combined liquid and vapour flux	[kg m^{-2} s^{-1}]
q_v	Moisture flux	[kg m^{-2} s^{-1}]
q_{vap}	Vapour flux	[kg m^{-2} s^{-1}]
r	Radii of meniscus	[m]
R	Gas constant	[J mol^{-1} K^{-1}]
t	Time	[s]
v	Water vapour content	[kg m^{-3}]
x	Coordinate	[m]
Z_v	Vapour permeation resistance	[s m^{-1}]
$Z_ø$	Vapour permeation resistance	[m^2 s kg^{-1}]
γ	Surface tension	[N m^{-1}]
$\delta(T, ø)$	Moisture transport coefficient	[kg m^{-1} s^{-1}]
δ_v	Moisture transport coefficient	[m^2 s^{-1}]
ΔP	Laplace pressure	[Pa]
η	Dynamic viscosity	[Pa s]
ρ_w	Water density	[kg m^{-3}]
$ø$	Relative humidity	[-]

Table of Contents

1 Introduction

1.1 Background

The reactor containment is one of the most important structures in a nuclear power plant (NPP), as the containment wall is the final barrier that protects the surrounding area from radioactive leakage, both during normal operation and in case of an accident. The main function of this structure is thus to envelop and protect the reactor vessel. There are several types of NPPs, and the design of the reactor containment can differ, both in size and shape. Two of the Nordic countries, Sweden and Finland, have nuclear power as an electric power source, as of 2015. The Nordic NPPs, which are in operation, were all built during the period from the late 1960s to the mid-1980s. Three different types of NPPs were in operation in 2015: boiling water reactor (BWR), pressurized water reactor (PWR) and water–water energetic reactor (VVER). The Nordic BWRs were designed by ASEA-Atom, the PWRs were manufactured by Westinghouse, and the VVER by Atomstroyexport.

The climatic condition, i.e. humidity and temperature, inside the containments is monitored continuously by the plant owners, mainly to monitor the conditions in specific zones close to sensitive equipment and to detect steam leakage. The climatic conditions inside the reactor containment may affect different mechanical components because of the moisture or temperate conditions. There are many building components, such as joints, fastening plates, pipe or cable lead-throughs, and other components that may be affected by climatic conditions. With a combination of high humidity and high temperature, surface condensation on cold surfaces may occur. Constant exposure of a metal surface to humidity may lead to surface corrosion. Thus, the climatic condition within the reactor containment is an area of importance for prediction of the life of the equipment.

The climatic conditions in the containments vary not only between different reactors and within each containment, but also with time. These variations will affect the concrete structures because of the interaction between the containment and the concrete components. The climatic conditions inside a reactor containment are affected by the boundary conditions. The boundary is defined as the contact zone between the air in the reactor containment and the concrete surfaces inside the containment. The humidity conditions inside the containment will, in addition, decide to what level the concrete structural elements will eventually dry when in equilibrium with its surrounding, a state not likely to be achieved over the technical lifespan of the containment.

The main source of moisture inside a containment is generally presumed, within the nuclear industry, to be water leaking from steam pipes. The other potential sources are, e.g. the suppression pool in the BWR and the large amount of concrete within the reactor containment. The air within the containments is dehumidified during operation; however, the amount of water extracted has not been well documented and/or is not accessible. This limits the possibility to derive and quantify the actual moisture contribution to the containment from potential sources. However, in this study, it is considered that concrete may have a notable effect, as it is a large moisture source.

The most widely used building material to construct reactor containments is concrete. Close to 95 % of the NPPs constructed between 1971 and 1999, worldwide, have some type of concrete containment [1]. Most of the containments are single-walled structures with prestressed concrete, or single-walled structures with only conventional reinforced concrete, or double-walled structures of conventional reinforced concrete with or without prestressing [1]. Both single-walled structures and double-walled structures are normally constructed with a steel liner to ensure leak tightness. The steel liner is either embedded in the concrete wall or installed on one of the concrete surfaces. When the steel liner is embedded, the wall is divided to an outer and an inner containment wall.

Apart from reasonably high compressive strength and good durability, which may be considered beneficial for a nuclear facility, there are additional properties or parameters relevant to a nuclear facility such as thermal conductivity, heat capacity [2], moisture transport coefficient, creep and shrinkage [3], gas permeability [4], and neutron and gamma radiation shielding properties [2, 5]. Most of these properties or parameters are dependent on the moisture content as well as on the water to cement ratio (w/c-ratio), degree of hydration, and cement type and content.

Moisture content in concrete has been studied in several fields for decades, mainly focusing on drying of concrete slabs and walls in buildings, e.g. [6, 7], the influence of moisture content on creep and shrinkage, e.g. [8-12] and degrading mechanisms such as alkali silica reactions [13] and frost related damage, e.g. [14, 15]. Most moisture related studies on concrete have been carried out in a laboratory controlled environment or as computer simulations; only a few studies have been based on environmental effects in the field, e.g. [16, 17]. No systematic measurements or studies on the moisture condition within reactor containments and internal concrete components have been presented. There are however a few studies where the moisture level has been estimated [5, 18] or measuring techniques have been evaluated [19]. Some measurements and models have also been made to primarily evaluate the conditions in the outer wall of a containment [18, 20-22]. These studies will be further discussed in *Section* 2.6.

Knowledge of the state of concrete structures in a reactor containment is important, especially for considering long-term operation. Because of the long-term exposure of the structures to high temperatures, it is necessary to evaluate how these conditions affect the concrete structures, and also whether the drying rate is sufficiently large to impact ambient

humidity. High temperatures in combination with low ambient relative humidity (RH) could result in a large transport potential for drying of the concrete.

The climatic conditions inside a nuclear reactor containment change over the years. How these changes affect the concrete structures within the containment, and whether the concrete itself affects the containment, have not yet been fully investigated. Thus, the knowledge of the moisture history and the possibility of predicting its development with time are of great value for assessing the current and future conditions of concrete structures.

1.2 Aim and research objectives

The aim of the research project presented in this thesis was to investigate and evaluate the climatic conditions inside nuclear reactor containments, historically, at present, and in future. Though the knowledge of the inner climate of a reactor containment and the condition of the concrete structure within the containment are important in order to evaluate their long-term effects on the containment, no studies dealing with climate conditions inside a nuclear containment have been carried out so far.

The main research objectives prior the project were the following.

I. Suggest and develop surveillance methods – i.e. measurement devices, measurement locations, data acquisition systems, etc. to determine the exposure conditions around the structural elements and the impact of these conditions on the structural elements.
   Chapter: 5 **Papers: III, IV, V**

II. Clarify the temperature and humidity conditions in the containments, by explaining and quantifying them.
   Chapters: 2, 5, 7 **Papers: I, II, III, IV, VI**

III. Compare the as-designed climatic conditions around the structural elements with the actual conditions and explain the differences between them. If necessary, suggest remedial actions to re-establish the as-designed conditions.
   Chapters: 2, 7 **Paper: VI**

IV. Determine whether there are any differences between two containments of the same type with regard to temperature and moisture conditions, and explain the reason for the differences.
   Chapters: 2, 5, 6, 7 **Papers: II, III, IV, VI**

V. Determine the moisture flow inside and through concrete structures and quantify the possible consequences.
   Chapters: 3, 4, 6, 7 **Papers: II, IV, VI**

VI. Develop guidelines for new build in order to avoid differences between the prescribed conditions and working conditions.
   Chapter: 2, 7 **Paper:**

2 Nuclear power plant

A nuclear power plant refers to a nuclear reactor that produces electric energy; research facilities and facilities designed for district heating are not included in this study.

There are several different NPP types worldwide; the most common type is the PWR, followed by the BWR [1]. Large variations in design exist within each type. In this thesis, only the Nordic PWRs and BWRs are considered.

Sweden and Finland are the only two Nordic countries that have nuclear power as an electric power source, as of 2015. In 2015, there were 14 NPPs in operation, one was under construction and two have been decommissioned (Barsebäck 1 and 2). In Sweden, there were ten NPPs in operation, distributed over three nuclear power sites. Ringhals, which is the biggest site, has four reactors, consisting of one BWR and three PWRs. The other two sites in Sweden are Forsmark and Oskarshamn. The reactors in these sites consist of three BWRs each.

Finland has two nuclear power sites, Olkiluoto and Loviisa. In Olkiluoto, there are two BWRs in operation and one additional evolutionary power reactor (EPR) under construction. At Loviisa, there are two VVERs; these two reactors are not included in this study.

Most of the reactors in Sweden and Finland have one or more similar reactors on site or at another Nordic site. Figure 1 shows the family tree of the NPPs at Ringhals, Forsmark, Oskarshamn and Olkiluoto, and the two reactors at Barsebäck that have been shut down.

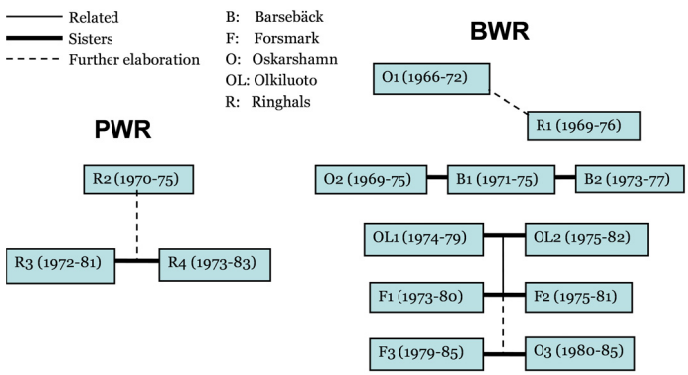

Figure 1. Family tree of the Swedish and Finnish BWRs and PWRs with the construction start year and commercial operation start year within parentheses

Only four of the Nordic NPPs were further evaluated in this work. The reactors were chosen to represent four of the five different groups, as presented in Figure 1. The PWRs are represented by Ringhals 4; Ringhals 1 represents the old generation BWR, Forsmark 2; the four Swedish and Finnish BWRs and Forsmark 3 represent the newest BWRs.

2.1 Reactor safety

The reactor building and the structures within are the main structures at an NPP. Depending on the reactor design, the reactor building can be either the building envelope housing the reactor containment, or the actual containment itself. The main purpose of the reactor containment is the following, according to the International Atomic Energy Agency (IAEA) [23].

- Isolate radioactive substances during operation and in the event of an internal and/or external accident.
- Protect the NPP from natural and human induced events.
- Shield radiation during operation and in accidental conditions.

Safety is the main focus at an NPP, and the strategy for safety is called defence in depth [24]. The strategy consists of five levels of safety, with the principle that if one level fails, the next will take over. The main objective is to prevent accidents, but if the prevention fails, the strategy is designed to limit the potential consequences and prevent any development into more serious conditions. Level 1 in the defence strategy corresponds to prevention of abnormal operation through conservative design and high quality, while Level 5 corresponds to the situation when the containment fails with significant release of radioactive material as a consequence [24].

In general, there are four main barriers designed to prevent leakage and spreading of the radioactive material; the fuel, fuel rods, reactor vessel, and reactor containment. For some NPPs, such as the Nordic BWRs, the reactor building is considered as the fifth barrier, as shown in Figure 2.

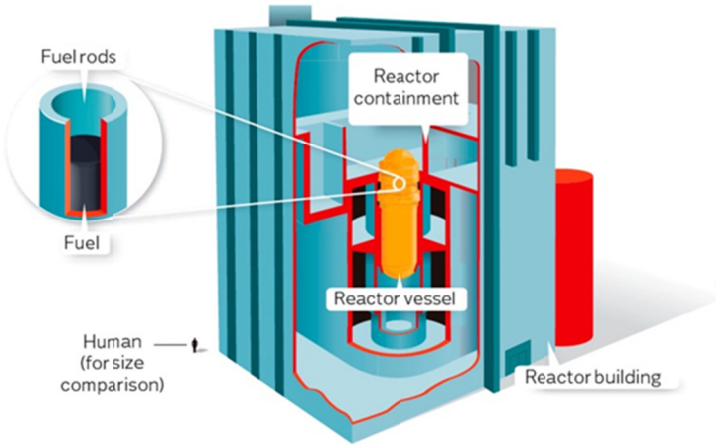

Figure 2. The four main safety barriers for preventing leakage of radioactive material to the surroundings during operation and in the event of an accident. If the NPP has a reactor building envelop outside the containment, this can be considered as the fifth complementary barrier. (Figure owned by Vattenfall AB, published with their permission)

The reactor containment is the last main barrier, and the structure has to contain and control the radioactive material if the other barriers fail. This makes the reactor containment one of the most important structures in an NPP.

Leakage of radioactive material to the surroundings is the primary risk in case of an accident. The possible accidents can be divided into two main groups, internal and external. The external accidents are, earthquakes, flooding, tsunamis, extreme cold or heat, tornadoes (with flying debris), airplane crash, etc. In these cases, the containment has to ensure that the leak tightness is not jeopardized. External accidents may also be a factor that induces an internal accident, e.g. because of a station black out.

The main internal accidents or events can be subdivided into five categories [25].

- Break in high energy systems
- Break in systems containing radioactive material
- System transients causing representative limiting loads (e.g. pressure, temperature or dynamic loads)
- Containment bypass events such as loss of cooling accidents (LOCA) in interfacing systems or steam generator tube rupture
- Internal hazards

An LOCA is considered as a basic accident condition for a reactor containment [1]. One possible scenario when an LOCA can occur is when one of the pipes in the primary circuit breaks. In this scenario, the pressure and temperature inside the containment increase rapidly, affecting the reactor containment with a high internal pressure. The water level inside the reactor vessel drops, and if the safety systems which are expected to maintain the

cooling of the core fail, there is a risk of core melt accident, making the event a serious accident with high temperature and high internal pressure.

If the containment is not leak tight, an LOCA-scenario could result in a leakage of radioactive material to the surroundings. In a PWR, depending on the containment design, an LOCA normally generates a pressure increase of approximately 0.5 MPa and a peak temperature of 150 °C. For a BWR, the corresponding pressure is 0.6 MPa and the temperature is 170 °C [1]. The leak tightness of the Nordic containments is tested thrice during every ten-year period to ensure that the structure can handle the high pressure.

The strategies to control the pressure increase vary depending on the reactor design. The PWRs used in Sweden employ a design concept called full pressure dry containment. To withstand the increased temperature and steam build-up, the containment has a large volume, and thus the pressure increase is limited without jeopardising the structure and leak tightness.

The BWRs in Sweden and Finland use a pressure suppression containment system. The containments are divided into two main compartments, drywell and wetwell, connected with several downcomers. In the wetwell, there is a suppression pool in which the downcomers are submerged. In case of a steam leakage in the drywell, the steam will be forced down into the suppression pool for condensation, thus reducing the pressure.

In the event of a core melt accident, the fuel cladding around the fuel melts, and hydrogen is produced. To avoid the risk from oxy-hydrogen gas, the air in the BWRs is replaced by nitrogen when the plant is in operation. In a PWR, the total space of the reactor containment is big enough so that a dangerous concentration of the gas cannot occur. In addition, the Swedish and Finnish reactors have an emergency ventilation system that can filter the radiation from the gas, thereby lowering the risk from oxy-hydrogen gas and decreasing the pressure within the containment in case of an accident.

As a result of nuclear reactions within the reactor core, different types of radiations are produced. To lower the radiation within the NPP, different types of radiation shields are used. Different materials have varying abilities to shield radiation. Apart from materials such as lead and steel, concrete is a suitable material owing to its high density and the presence of internal water.

The neutron and gamma radiation shielding properties have been investigated in several studies [2, 5, 26-33], often with the attended use in nuclear facilities. The major forms of radiation that escape from the reactor core are high-energy gamma rays and neutron radiations. The reactor vessel absorbs most of the energy from the radiations, and most of the remaining radiation is thereafter absorbed in the biological shield.

The neutron attenuation in concrete is due to the chemical composition of the hydrated cement, and mainly the amount of hydrogen. Because of this, the attenuation is strongly dependent on the moisture content in the concrete, the main source of hydrogen in concrete. One example of the moisture influence is stated by Thorn in 1961, who showed

that lowering of moisture content in concrete by five percentage points increases the relaxation length by 30 % [2].

Gamma ray shielding does not depend on the moisture content in the same way as neutron radiation. The shielding property that affects the gamma ray radiation attenuation is the density of the material. Test results with radiation at 3 MeV (mega-electron volt) show that the gamma ray relaxation length increases by the same magnitude as the inverted moisture loss due to drying [2].

2.2 Pressurized water reactor

The PWR is the most widely used reactor type in the world. The fundamental principle of the reactor function is shown in Figure 3, which illustrates the primary and secondary circuits. The primary circuit includes the reactor vessel, which produces overheated pressurized water through nuclear fission. In the secondary circuit, the pressurized water is used to produce steam, which is used to propel the turbines and generate electrical energy.

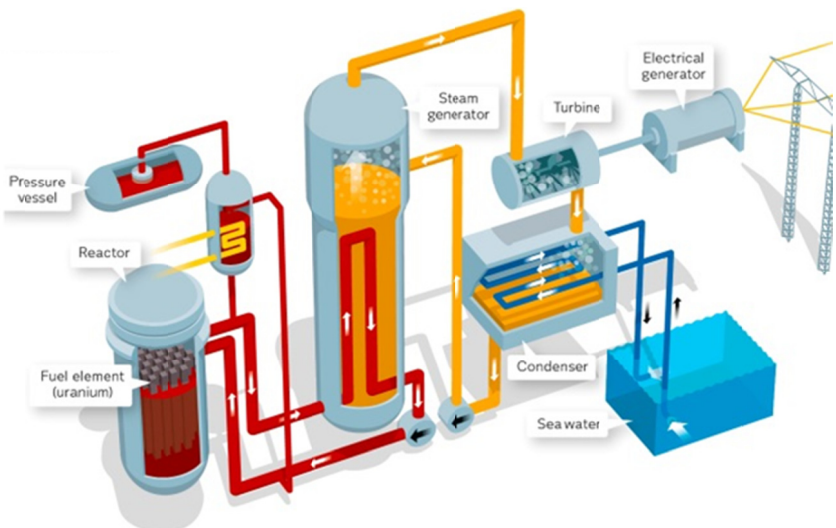

Figure 3. Reactor design and basic function of a PWR. The PWR is divided into two circuits, one where pressurized water is produced in the reactor and the other which uses the water to produce steam to propel the turbines in the steam generator. (Figure owned by Vattenfall AB, published with their permission)

Both the primary circuit and the steam generator are located within the reactor containment in a PWR, thus requiring a large volume. This is well adapted to the full pressure dry containment design strategy, as mentioned in *Section* 2.1, which also requires a large volume. The total volume within the PWR containment at Ringhals 4 is

approximately 55,000 m^3, and most PWRs around the world have an inner volume of approximately 60,000 m^3 [1].

For single-walled full pressure dry containments, there is normally no building envelope housing the containment; instead, the containment wall is exposed to the outdoor climate. The Nordic PWRs have a single prestressed, 1.1 m thick, concrete containment wall with an embedded steel liner located approximately 300 mm from the inner surface to ensure leak tightness. The outer part of the wall (outer containment wall) is both horizontally and vertically prestressed. The inner containment wall is made of reinforced concrete.

Apart from the inner containment wall and the bottom slab, there are a vast amount of internal concrete structures, including the fuel handling pool and load bearing walls, and columns for the internal components, e.g. steam generators and pressurizer. Around the reactor vessel, which is located in the lower part of the containment, there is a biological shield. The thickness of the shield can vary for different reactors, but for the Swedish reactors, they are approximately 2 m thick. The total concrete volume within the steel liner is 8000 m^3 for the Nordic PWRs. Figure 4 illustrates the section of a PWR, based on Nordic PWRs.

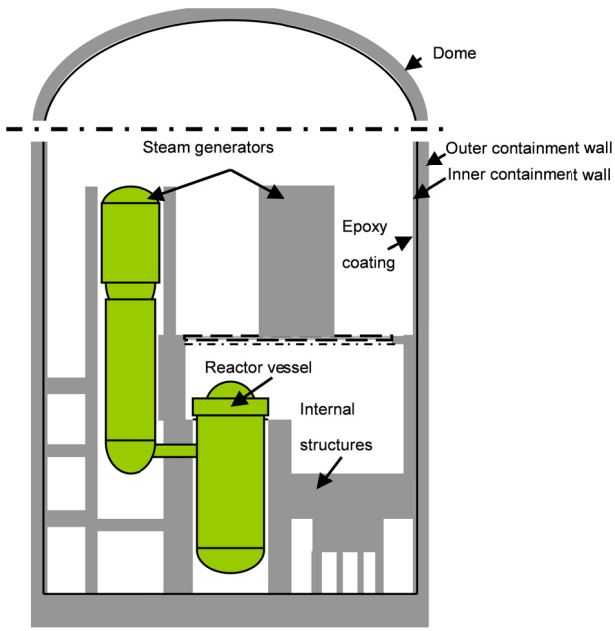

Figure 4. Schematic illustration of a PWR. The illustration is not to scale, but only an illustration of the general design. The thick black lines represent the steel liners and the grey surfaces represent the concrete.

2.3 Boiling water reactor

The boiling water reactor BWR is the second most common reactor type in the world. The reactor design is based on one primary circuit where the steam is produced directly in the reactor vessel and later used to propel the turbines. An illustration of the basic principle of a BWR is given in Figure 5.

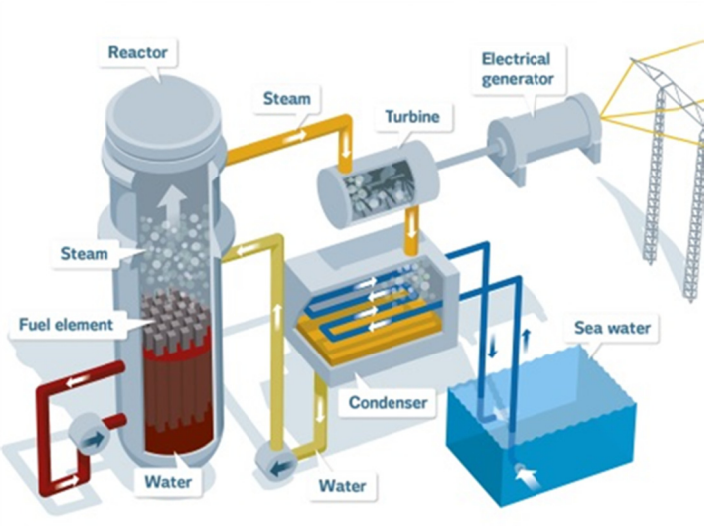

Figure 5. Reactor design and basic function of a BWR. In a BWR, steam is produced directly in the reactor and later used to propel the turbine in one primary circuit. (Figure owned by Vattenfall AB, published with their permission)

Because of the pressure suppression design, as described in *Section* 2.1, the BWR containment can be significantly smaller than large dry containments such as the Swedish PWRs. A typical BWR containment has a volume of approximately 12,000 m^3 [1].

The Nordic BWRs are all located within a building envelope, i.e. the reactor building, protecting the containment from external sources. The containments are all made of prestressed single-walled concrete with embedded steel liners. Normally, the walls are approximately 1.1 m thick, and the steel liner is located approximately 300 mm from the inner surface. The steel liner is used to ensure leak tightness of the containment.

The reactor containments are cylindrical, and the inside region is divided into two main compartments, drywell and wetwell. The drywell is the main compartment housing the reactor vessel and main components. Around the reactor vessel, there is a biological shield made of prestressed or reinforced concrete. The thickness of the biological shield varies for the different reactors, but normally it is approximately 1–2 m. The compartment below the reactor vessel is considered to be a part of the drywell, and is normally called the lower drywell.

The upper drywell is separated from the wetwell by an intermediate floor. The suppression pool is located in the wetwell. The pool consists of deionized water, and the pool walls are covered with stainless steel sheets. The upper parts of the wetwell, above the water line, do not have a steel covering. The inner wall that separates the wetwell and the lower drywell consists of reinforced concrete with a thickness of approximately 800 mm. In total, the BWRs contain approximately 2000–2500 m^3 of concrete, with the steel liners located within the concrete. Figure 6 presents an illustration of a BWR containment design.

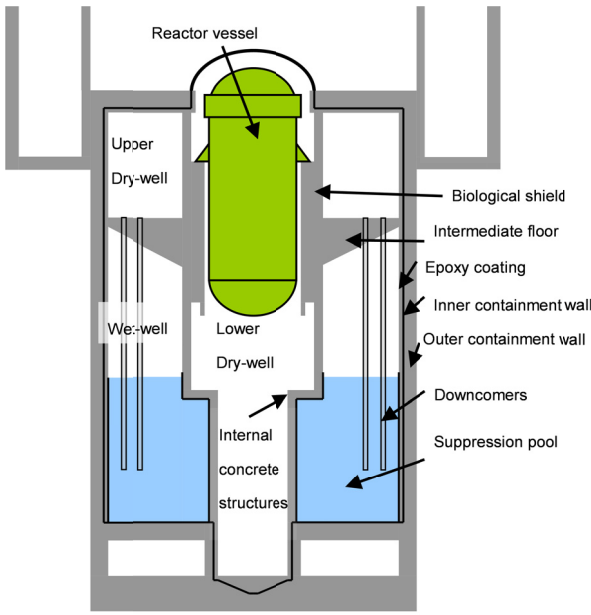

Figure 6. Schematic illustration of a BWR. The illustration is not to scale, but only an illustration of the general design. The thick black lines represent the steel liners and the grey surfaces represent the concrete.

2.4 Nordic reactor containments – similarities and differences

The design of the inner containment wall of all the Nordic reactors considers similar functional requirements. The inner containment wall is designed to protect the steel liner from internal missiles as well as from degradation. Because the inner containment wall in each containment covers a large part of the total volume, a comparison between them gives a good overview of the overall similarities and differences regarding the concrete structures. In Table 1, the inner containment walls from four reactors are presented with the data from IAEA [34], Roth et al. [35] and construction drawings and personal communications with

the personnel at Forsmark and Ringhals. The amount of concrete and the inner volume were both rough estimations based on the construction drawing.

Table 1. Comparison of the inner containment walls at four reactors with regard to the year of start of construction and the year when first put into commercial operation, the reference unit power (RUP) as of 2011 [34], the reactor containment, RC, wall thickness, cement content, cement type, w/c-ratio, inner volume and total amount of concrete located inside of the steel liner. This information was gathered from construction drawings, personal communications, IAEA [34] and Roth et al [35]. Cem I, LH and STD correspond to ordinary Portland cement concrete, low heat cement and standard cement, respectively. The cement originated from the abandoned Limhamn cement factory, Scania, Sweden.

	Constr. start / in operation	RUP MW(e)	Inner RC wall thickness [mm]	Cem. content [kg m^{-3}]	Cem.type	w/c-ratio [kg kg^{-1}]	RC air Volume [m^3]	Tot. Conc. amount within liner [m^3]
R 1	1969 / 1976	854	330	365	CEM I STD	0.42	13000	2000
R 4	1973 / 1983	945	330	365	CEM I LH	0.42	55000	8000
F 2	1975 / 1981	990	260	370	CEM I LH	0.46	13300	2500
F 3	1979 / 1985	1170	300	*c.*370	CEM I LH	0.42/0.43	15500	2300

A comparison of the water/cement-ratio (w/c-ratio) or the cement content in the inner containment wall in the four containments shows no significant trend over time or between two sites. The inner containment walls are fairly similar, considering the type and the amount of the cement used (approximately 365–370 kg m^{-3} ordinary Portland cement). All four inner walls were constructed with old Swedish concrete classification K50 [35], roughly equivalent to concrete class C40/50, as defined in EN206-1. A comparison of the concrete to space volume ratio shows fairly similar results between all four reactor containments with a ratio of approximately 1:6. Only the concrete to space volume ratio at Forsmark 2 had a significant difference with a ratio of 1:4.5.

2.5 As-designed climatic conditions

As far as the structural parts are concerned, it was found that concrete temperature is the only climatic condition that is regulated in the design codes regarding reactor containments and concrete in NPPs. The Nordic countries used the American concrete Institute (ACI) 349 and 359, Code Requirements for Nuclear Safety-Related Concrete Structures [36, 37], when constructed.

In normal operation, the highest long-term concrete temperature allowed is 150 °F (approximately 66 °C). However, in local areas, e.g. around steam pipe penetrations, the temperature is allowed to be higher, i.e. up to 200 °F (approximately 93 °C). It is possible to increase these temperature limits, if tests show that the strength of the concrete is not lowered under the accepted design criteria because of the increased temperature. Tests should also provide evidence that the elevated temperatures do not cause deterioration of concrete [36].

There are also regulations regarding accident inflicted temperatures or short term temperatures. In these cases, the concrete surface temperature shall not exceed 350 °F (approximately 176 °C). In local areas, however, the concrete surface is allowed to reach up to 650 °F (approximately 343°C) from steam or water jets in case of a steam pipe failure [37].

No recommendations regarding RH levels have been found for the climatic conditions inside the nuclear reactor containment as well as for the moisture content or RH in concrete components. IAEA [25] has, however, recommendations to monitor the humidity levels in the containment during operation, e.g. to detect leakage from the primary circuit.

Because the air within the reactor containments is dehumidified during operation, it is further assumed that the conditions measured within the containments are "as-designed conditions". However, details regarding the dehumidification of the reactor containment air were not found or accessible.

2.6 Actual climatic conditions

The climatic condition in the Swedish reactor containments has previously been studied primarily with regard to the drying of the outer containment wall, both on BWRs and PWRs [18, 20, 21, 38]. In these studies, the ambient conditions outside of the outer containment on three reactors were monitored during operation. The results showed that the temperature at the surface varied at different heights in the BWR, with temperature of approximately 50 °C high up and 20 °C down below. The results also showed that the vapour content inside the reactor building followed that of the outdoor conditions. This resulted in low RH at higher levels on the containment wall and significantly higher RH at lower levels. The results also showed that when compared to the temperature inside of the containment, there was no significant temperature gradient in the containment wall [20]. In contrast to the BWR, the measurements at the PWR showed that there were large temperature gradients on those sections of the containment wall that were exposed directly to the environment [20].

A model was developed and applied to the BWR and PWR containments. The model was validated using measurements on concrete cylinders, extracted from the outer containment wall at one of the BWRs [38] and measurements on the outer surface of the containment

wall [20]. The model showed good agreement with the measurements, and the moisture profile in the containment concrete indicated high humidity at greater depths [18]. The model was also applied to the PWR containment wall; however, it was not validated at greater depths [21]. The moisture profile at the PWR containment wall was predicted to decrease with depth owing to the temperature gradient effect on the moisture transport.

As the first step of the work presented in this thesis, the moisture profile was measured with respect to the degree of capillary saturation. The measurement was done on concrete from inner and outer containment walls at the PWR Ringhals 4 **(Paper I)**. The results presented in **Paper I** show a clear moisture gradient in both inner and outer containment walls, with high moisture levels at greater depths. These results indicated that the model presented in the previous study [21] did not properly describe the influence of temperature gradient, a conclusion later stated by the same author [39].

The earlier studies showed that the temperature and RH varied within the reactor containments. Temperatures of 20–60 °C and RH of 30–60 % were observed in BWRs during operation. The measurements within a PWR showed that the temperature on low levels was in the range of 20–30 °C with a corresponding RH of approximately 50 %, while the temperature higher up was approximately 40 °C with an RH of approximately 30 % [21].

An evaluation of the potential factors that may have a significant influence on the internal temperature and humidity variation during operation is presented in **Paper II**. Measurements of temperature and RH in the two reactor containments, one BWR and one PWR, with the measurement setup developed in this project, were compared with respect to three identified factors: outdoor temperature, NPP cooling (i.e. seawater temperature), and the operational state of each reactor. The conclusions drawn in **Paper II** were that only the outdoor temperature had a significant influence on the conditions in the PWR. No clear correlation to the seawater temperature or the operational state (power outage not included) was found in the PWR or the BWR. The conclusion drawn from the studies was that the conditions within a BWR should be stable over the years without any significant difference, while the conditions within a PWR may change from year to year depending on the ambient conditions, as well as with daily and seasonal changes. The measured conditions as well as the seasonal trends as observed in **Paper II** are also found in the work by Nilsson and Johansson [21].

In this project, the actual conditions in four reactor containments, both in the concrete as well as in the surroundings, were measured and evaluated. Evaluations of the measuring technique and setup, as well as the measured results are presented in **Papers II**, **III**, **IV** and **VI**. The setup and the results are also briefly presented in Chapter 5.

3 Moisture transport

Moisture transfer in a porous material is a combination of different transport phenomena. When describing the transport on a microscale or nanoscale, the transport is often divided into permeation of liquid water, permeation of gaseous phase, diffusion of water vapour in gas [40], inter layer water transport and transport in adsorbed water [39]. Gravity induced transport may be neglected while considering porous media with very small pores [41] such as concrete. While considering the transport on a macro level, one can combine the different flows to liquid and vapour flow [39, 42-46]. While using a macroscopic approach, the material can be considered as a quasicontinuum; thus, it is possible to use volume average quantities in the model [47]. This also allows the moisture flow [kg s^{-1}] to be expressed as flux [kg m^{-2} s^{-1}] for porous materials.

Vapour flux is often described through diffusion, i.e. the motion of moisture molecules due to difference in concentrations. The motion is randomized, but the total vapour flux can be described using Fick´s first law of diffusion, as given in Eq. 1.

$$q_{vap.} = -D_c \frac{\partial c}{\partial x} \tag{1}$$

where

$q_{vap.}$	[kg m^{-2} s^{-1}]	Vapour flux
x	[m]	Coordinate
D_c	[ ]	Diffusion coefficient
c	[ ]	Transport potential

The unit of diffusion coefficient is dependent on the unit of transport potential, and hence, they may be expressed in several ways.

The transport potential c for vapour transport can be described with any of the state variables–RH, water vapour content v, moisture content w, water vapour pressure p, or pore water pressure P_w. When in isothermal condition, the transport potential can be redefined because of the unique relations between the state variables [48] through the material specific sorption isotherm and the relation described in the Kelvin equation when combined with the Young–Laplace equation, given by Eq. 2.

$$P_w = \frac{RT\rho_w}{M_w} \ln \phi \quad (2)$$

where

P_w	[Pa]	Pore water pressure
ø	[-]	RH
R	[J mol^{-1} K^{-1}]	Gas constant
M	[kg mol^{-1}]	Molar mass of water
ρ_w	[kg m^{-3}]	Water density
T	[K]	Temperature

Liquid transport in a porous material can be divided into viscous saturated flux and capillary transport. Both can be described by Darcy's law. The viscous flux is valid only if there is a pressure gradient over the structure. The viscous flow is neglected in this study. The transport potential for capillary transport is the Laplace pressure ΔP, as given by Eq. 3.

$$q_{liq.} = -\frac{k_p}{\eta}\frac{\partial \Delta P}{\partial x} \quad (3)$$

where

$q_{liq.}$	[kg m^{-2} s^{-1}]	Liquid flux
k_p	[kg m^{-2}]	Effective permeability
η	[Pa s]	Dynamic viscosity
ΔP	[Pa]	Laplace pressure
x	[m]	Coordinate

The pore water pressure, given by Eq. 4, is further defined in a capillary pore as the difference between the atmospheric pressure and the pressure difference over the meniscus, i.e. Laplace pressure, as described according to Young–Laplace equation (Eq. 5).

$$P_w = P_{atm} - \Delta P \quad (4)$$

$$\Delta P = \gamma\left(\frac{1}{r_1} + \frac{1}{r_2}\right) \quad (5)$$

where

P_w	[Pa]	Pore water pressure
P_{atm}	[Pa]	Atmospheric pressure
ΔP	[Pa]	Laplace pressure
γ	[N m^{-1}]	Surface tension
r	[m]	Radii of the meniscus.

Normally, the atmospheric pressure P_{atm} (approximately 100 kPa) is much smaller than ΔP and can be neglected.

Combining Eqs. 2, 4, and 5 and expressing the RH with regard to water vapour pressure gives the following equation.

$$-\Delta P \approx P_w = \frac{RT\rho_w}{M_w} \ln\left(\frac{p}{p_s}\right) \tag{6}$$

where

ΔP	[Pa]	Laplace pressure
P_w	[Pa]	Pore water pressure
R	[J mol^{-1} K^{-1}]	Ideal gas constant
T	[K]	Temperature,
ρ_w	[kg m^{-3}]	Density of water
M_w	[kg mol^{-1}]	Molar mass of water
p	[Pa]	Water vapour pressure
p_s	[Pa]	Water vapour pressure at saturation.

The total moisture transport through a porous material is a combination of both vapour and liquid transport, which can be separated only in theory. The combined vapour and liquid transport can be described by combining Eqs. 1, 3, and 4; when P_{atm} is neglected, the total flux q_{tot} [kg m^{-2} s^{-1}] can then be expressed as Eq. 7.

$$q_{tot} = q_{vap.} + q_{liq.} = -D_c \frac{\partial c}{\partial x} + \frac{k_p}{\eta} \frac{\partial P_w}{\partial x} \tag{7}$$

In an isothermal state, it is further possible to rewrite the total flux equation (Eq. 7) to one single expression [49], as given by Eq. 8, considering Eq. 6. The diffusivity and permeability are then combined into one moisture transport coefficient δ_c, which describes both the vapour and liquid water transport resistances and one single moisture transport potential (c) for both vapour and liquid transport is used. The unit of δ_c depends on the unit of the transport potential.

$$q_{tot} = -\delta_c \frac{\partial c}{\partial x} \tag{8}$$

Further discussion regarding moisture transport in porous materials, and the required material properties in non-isothermal conditions and at different uniform and quasi-uniform temperature conditions are described in Chapter 4 and in **Paper VI.**

4 Determination of material properties

Concrete is a complex material with material properties that may vary over time. These variations can be due to various factors, e.g. ongoing cement hydration or moisture and temperature variations. To better describe the process within a cement-based material, identification and determination of these parameters have been done experimentally and theoretically for several decades. At least two material properties are needed to describe the moisture condition and moisture transport in a porous material. They are, moisture fixation, which is normally described with sorption isotherm, and moisture transport coefficient, which combines vapour and liquid transport of water in porous materials; however, the combination is valid only under isothermal conditions.

The accuracy of a moisture transport model in a specific concrete structure increases significantly if appropriate material properties are used. For this to be possible, measurements on that specific material or on an equivalent material will have to be done. However, if a large structure is considered, such as an inner reactor containment wall, which corresponds to almost 2000 m^3 of concrete for a PWR, variations can also be expected between different areas of the structure. Differences because of reasons, such as different castings, different concrete batches, and different climatic conditions, are possible, but were neglected in this study. Material variation depending on the depth of the structure is also a possibility. In a structure exposed to continuous drying and/or temperature gradient, internal variation should be possible because of the temperature and moisture dependency of cement hydration. This aspect was evaluated in this study through moisture transport coefficient measurements over the depth of the containment wall, and measurements of variation in the degree of hydration of the structure.

A model based on the mass conservation principle as presented in Fick's second law of diffusion was established through the model by Bažant and Najjar [50], and presented in **Paper VI** (Eq. 9). The material properties needed for the model were, moisture and temperature dependent moisture transport coefficient $\delta(T,ø)$ and the temperature and moisture dependent moisture fixation. The moisture fixation is given in Eq. 9 as the inverse slope of the sorption isotherm $k(T,ø)$.

$$\frac{\partial \phi}{\partial t} = k(T,\phi) div \left(\delta(T,\phi)\, grad\, (\phi + K(\phi) \frac{\partial T}{\partial t} \right) + K(\phi) \frac{\partial T}{\partial t} \quad (9)$$

where

ø	[-]	RH
t	[s]	Time
k(T,ø)	[m^3 kg^{-1}]	Invers slope of the sorption isotherm
δ(T,ø)	[kg m^{-1} s^{-1}]	Moisture transport coefficient
K(ø)	[K^{-1}]	Hygrothermal coefficient [51]
∂T/∂t	[K]	time dependent temperature change

Moisture transport within a material, as well as out of the material, is also dependent on the water vapour permeation resistance Z of the surface. In this study, this was considered through the properties of an epoxy coating, that was applied on all concrete surfaces within the containments. The composition of the epoxy coatings that were used in the different containments, their properties, and if there were any variations between the containments, were not known.

Four different NPPs were included in this study. The plants included in this study differed in age, and were located at two different geographic locations. The comparison presented earlier, i.e. in *Section* 2.4, Table 1, had shown that there are several similarities between the different plants regarding concrete compositions, cement type, cement content and w/c-ratio. Because of these similarities, it was assumed that using the material properties from one of these structures would be a better approach for simulating the moisture transport than using the already existing models or empirical regression models, e.g. those based on the moisture transport coefficient measurements done by Hedenblad [52]. All the material samples used in this study were collected from the containment wall at Ringhals 4. The material was gathered from a concrete block that was extracted from the wall during a steam generator change at Ringhals 4 in 2011.

The material investigation within this work is divided into four parts as given below.
1) Moisture and temperature dependent vapour permeation resistance of epoxy coating.
2) Moisture and temperature dependent moisture transport coefficient of concrete.
3) Desorption and adsorption isotherms of concrete.
4) Internal hydration variations.

The water vapour permeation resistance of the epoxy coating, given in *Section* 4.2, and the moisture transport coefficient for the concrete, given in *Section* 4.3, were evaluated using the cup method [7, 52]. To evaluate temperature dependency, measurements were done both at 20 °C and 50 °C.

The sorption isotherm measurements were planned and initiated using RH equilibrium climate box method. It should be noted that the measurements were aborted owing to measurement setup failure, and were discarded in this study. The intended approach was however as followed. Specimens of 10 mm thickness were first capillary saturated and then

placed in boxes with different levels of RH (held constant). Each climate box contained a CO_2 adsorbent and a different saturated salt solution to control the different levels of RH. One extra control box was prepared and used for confirming whether the equilibrium was reached. The specimens from the control box were measured until equilibrium was reached. Further, the specimens in the main boxes were measured only after equilibrium in the control box was reach. This was done to minimize disturbance on the main climate boxes. No results was obtained from the measurements due to the leakage from the climate boxes.

Internal variation within the concrete structure was evaluated through moisture transport coefficient measurements, which was done at four different depths and by evaluating the variations in the degree of hydration, as given in *Section* 4.4. The degree of hydration was evaluated by quantifying the calcium hydroxide variations over the depth of the structure through thermogravimetric analysis (TGA).

The findings collected from the material study were used in the moisture transport model (Eq. 9) and presented in **Paper VI** and Chapter 6. Because of failure of the setup, the sorption isotherm measurements on concrete with w/c ratios of 0.4 and 0.5, as presented by Nilsson [7], were used. Simulation was conducted assuming a linear relation between the two desorption isotherms, i.e. desorption isotherms for concrete compositions with w/c-ratios of 0.42 and 0.46, respectively. The temperature dependency of the moisture fixation was considered with regard to the hygrothermal coefficient, as presented in **Paper VI**.

4.1 Material

Forty concrete cylinders with a diameter of 94 mm and a length of 300 mm were extracted from a 6×8 m^2 concrete block from the containment wall at Ringhals 4. The concrete block was earlier removed because of a steam generator replacement in 2011. Figure 7 shows the inner side (inner containment wall) of the concrete block after the concrete for the material study was extracted. The specimens were extracted approximately four weeks after the concrete block had been removed from the containment wall. During that period, the concrete block was stored outdoors. The larger holes, as seen in Figure 7, and two additional holes from the outer containment wall, were used for measuring the degree of capillary saturation, as presented in **Paper I.**

The concrete composition is presented in Table 2, and the cement clinker composition of Low Heat (LH) cement from the disused Limhamn cement factory in Scania, Sweden, is presented in Table 3. The cement clinker composition may vary to some extent over time, but the variation should be within the region as presented in Table 3. The concrete at Ringhals 4 is fairly similar to that used in the other NPPs included in this study (see *Section* 2.4).

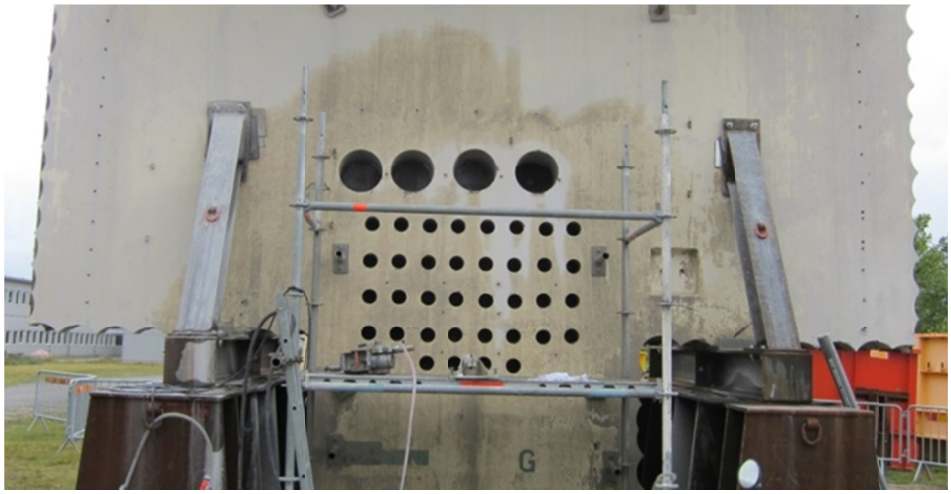

Figure 7. Concrete block from the containment wall at Ringhals 4 after the concrete cylinders were extracted from the inner containment wall

Table 2. Concrete composition of the inner containment wall at Ringhals 4 [35]

Cement type	Cement [kg m^{-3}]	Water [kg m^{-3}]	w/c-ratio	Gravel and sand [kg m^{-3}]	Stone [kg m^{-3}]
LH Limhamn	365	154	0.42	752	1135

Table 3. Cement clinker composition of LH Limhamn cement, data from Cementa AB 1979-10-22. Further description of the cement clinker is found in *Section* 4.3.

Alite (C3 S)	Belite (C2 S)	Celite (C3 A)	Ferrite (C4 AF)	Free CaO	Gypsum	Specific surface [m^2 kg^{-1}]
35	46	-	11	0.3	4.8	366

The concrete samples were core drilled, and water was used for cooling. The positions of the holes were chosen so that the amount of reinforcement in the samples was minimized. After extraction, the concrete samples were wrapped in plastic and transported to the laboratory at Division of Building Materials, Faculty of Engineering, Lund University. The ø94-mm cylinders were stored indoors, wrapped in plastic, for approximately five months before the test specimens for the different tests were prepared.

Each test specimen from the ø94-mm cylinders was sawed out from the cylinders by using a diamond blade with water cooling. The specimens were taken from different depths and with different thicknesses, as presented in Table 4. The naming of the specimens was based on: the depth from where the specimens were taken, (A-**D**): if the specimens where exposed for elevated temperatures, (H), or neutral temperatures (N or no letter): and if the surface specimens had an Epoxy coating, (E), or not.

Table 4. Description of the test specimens and test conditions for each test setup. The moisture transport measurements were made in different climates, one at 20 °C (1) and the other at 50 °C (2).

	Core Diameter [mm]	Specimen Thickness [mm]	Specimen Depth [mm]	Temp. [°C] (1)	(2)	RH [%]: Ambient (1)	(2)	RH [%]: Cup (1)	(2)	No.
Epoxy: Vapour resistance	94	10	0–10	20	50	55	10	75 85 98	74 81 96	36
Moisture transport coefficient	94	20	40–60 100–120 230–250	20	50	55	10	33 75 85 98	- 74 81 96	63
Amount of CH	94	10	40–50 150–160 250–260	-		-		-		9

4.2 Moisture transport properties

The moisture transport coefficient of the concrete and the vapour resistance of the epoxy were determined in steady state isothermal conditions, using the cup method. The cup method has been used earlier in several studies on porous materials such as concrete, but with different setup designs, e.g. [7, 48, 52, 53]. The setup used in this study consisted of a glass cup with an inner diameter of 92 mm and a height of 65 mm, and the method was designed similar to the one presented earlier by Nilsson [7]. Figure 8 shows a schematic illustration of the cup setup.

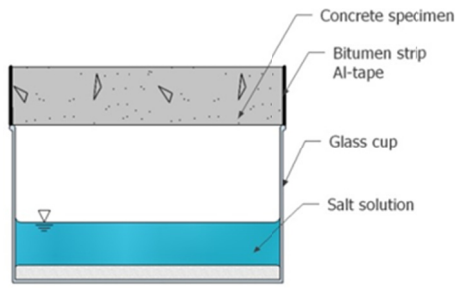

Figure 8. Schematic illustration of the cup method setup for measuring the moisture transport coefficient for concrete. The conditions within the cup are controlled with different saturated salt solutions.

The cylindrical surface of the test specimens was sealed with a heated bitumen strip before the cups were assembled. The strip was approximately 2 mm thick and had an aluminium foil on the outer surface. The strip was heated in 105 °C for approximately 45 s and pressed on to the concrete surface to ensure that the surface was properly sealed.

The cylinder specimen was placed on the glass cup, and two layers of aluminium tape were applied on the bitumen strip and the glass cup, as shown in Figure 9, to fasten the specimen and to create a hermetically sealed compartment under the specimen. The average air gap between the solution surface and the specimens was 40 mm.

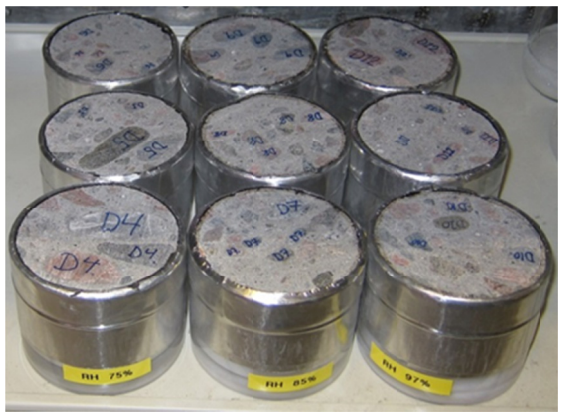

Figure 9. Nine of the specimens used for determination of moisture transport coefficient by the cup method.

Four different saturated salt solutions, as presented in Table 5, were used to establish different equilibrium level of RH with the cups. The different saturated salt solutions were defined with respect to the corresponding equilibrium RH, as presented by [54], at 20 °C and 50 °C.

Table 5. RH from saturated salt solutions at 20 and 50°C [54]

	20 °C	50 °C
$MgCl_2$	33.07 ± 0.18 %RH	
NaCl	75.47 ± 0.14 %RH	74.43 ± 0.19 %RH
KCl	85.11 ± 0.29 %RH	81.20 ± 0.31 %RH
K_2SO_4	97.59 ± 0.53 %RH	95.82 ± 0.45 %RH

The RH values presented in Table 5 are the values obtained at the surface of the saturated salt solutions. However, because of the diffusivity of air and the space between the surface of the saturated salt and the concrete specimen, the RH at the specimen would be lower. The diffusivity in air is temperature dependent, and at 20 °C it is approximately 25×10^{-6} m^2 s^{-1}, and the corresponding value at 50 °C is approximately 30×10^{-6} m^2 s^{-1} [55].

When the cups are in steady state condition, the moisture transport from the surface of the saturated salt to the specimen is equal to the moisture flow through the specimen. The ΔRH over the air gap can then be determined by Fick´s first law, as given in Eq. 1. Further reduction of RH at the specimen surface due to resistance at the saturated salt solution surface and at the specimen surface can be negligible according to earlier studies [7, 56].

To validate the tightness of the assembly, three validation cups were prepared. The specimens were 20 mm thick aluminium pucks with a diameter of 94 mm. Bitumen strip and aluminium tape were applied in the same manner as for the concrete specimens. The bitumen strip only covered 10 mm of the aluminium part to represent both the concrete and the epoxy coated specimens, as a conservative approach. Deionized water was used in the cups to give humidity at the water surface of approximately 100 %RH. High RH was chosen to increase the transport potential. It was assumed that the vapour resistance of the sealing was independent of humidity; thus, only one RH gradient was studied.

The validation specimens were placed in a climate chamber with 55 %RH and 20 °C. The mass change of the specimens varied up and down by a few milligrams during the measurement period. After seven months, the mass varied between two and five milligrams from the original mass. This proves that the validation setup was close to hermetically sealed condition. It should however be noted that a potential leakage between the bitumen strip and the concrete specimens has not been adequately tested, as the aluminium surface is much smoother than the concrete surface. Any effect form this factor was not considered in this study.

The moisture transport coefficient of the concrete was determined using a coupled vapour and liquid transport model, as given in Eq. 8, based on the mass change measurements and with water vapour content as transport potential (Eq. 10). Steady state flow was obtained over the cups at equilibrium when a constant time dependent loss of mass of the specimens was obtained. By measuring the loss of mass of the specimens over a prolonged period of time, the steady state mass change could be expressed as moisture flux q [kg m^{-2} s^{-1}], considering the specimen surface area. The measurements were made at different RH intervals, which could be translated into different water vapour contents v. Together with the thickness of the specimens, this gave the moisture gradient dv/dx. The quotient of moisture flux divided by the corresponding moisture gradient gave the moisture transport coefficient δ_v [m^2 s^{-1}] in that specific RH interval.

$$q_v = -\delta_v \frac{\partial v}{\partial x} \tag{10}$$

where

q_v	[kg m^{-2} s^{-1}]	Moisture flux,
δ_v	[m^2 s^{-1}]	Moisture transport coefficient (v)
v	[kg m^{-3}]	Water vapour content
x	[m]	Coordinate

A model earlier proposed by Anderberg and Wadsö [56] was used to determine the average moisture transport coefficients in the overlapping RH intervals from the measurements, as given by Eq. 11.

$$\overline{\delta_{12}} = \frac{\overline{\delta_{02}}(v_2 - v_0) - \overline{\delta_{01}}(v_1 - v_0)}{v_2 - v_1} \tag{11}$$

where index 0 represents the ambient vapour condition, and 1 and 2 represent the two vapour conditions in each cup. The model enables a more detailed analysis of the moisture dependency of moisture transport coefficient moisture dependency.

Hedenblad had previously determined the moisture transport coefficients of several different concrete compositions [52]. The earlier results of Hedenblad show that concrete with a w/c-ratio of 0.4 has a moisture transport coefficient of approximately 1.3×10^{-7} m² s^{-1} in the region of 33 to 65 %RH. The corresponding moisture transport coefficient for a concrete with a w/c-ratio of 0.5 is approximately 1.4×10^{-7} m² s^{-1}. The RH dependent moisture transport coefficient of concrete with a w/c-ratio of 0.4 is presented in Figure 10. The data is based on the measurements by Hedenblad and presented together with an approximated function, as given by Eq. 12. The equation is based on the function presented by Åhs [22], but it is adapted to fit the result by Hedenblad for a concrete with a w/c-ratio of 0.4 instead of 0.5 as for the function by Åhs. The function shows good agreement in the interval 30–90 %RH. Above 90 %RH, the function will overestimate the moisture flow. A more accurate correlation of the measured results can be obtained by means of curve fitting based on nonlinear optimization.

$$\delta_v = 1.3 \times 10^{-7} \cdot e^{2.455 \cdot \phi^{5.35}} \tag{12}$$

where

δ_v	[m² s^{-1}]	Moisture transport coefficient (v)
ø	[-]	RH

The first term represents the water vapour content dependent moisture transport coefficient in the lower RH interval, < 65 %RH, as reported by Hedenblad.

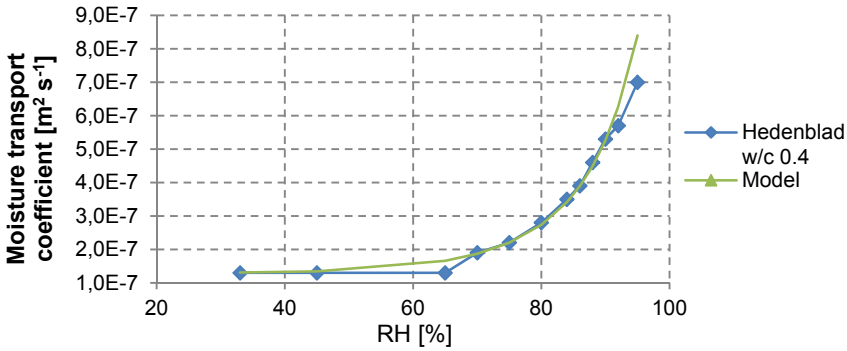

Figure 10. Moisture transport coefficient of concrete with a w/c-ratio of 0.4, based on measurements by Hedenblad [52], and the corresponding model (Eq. 12)

4.2.1 Epoxy vapour permeation resistance

The water vapour permeation resistance of the epoxy coating used on the concrete surfaces in the containments has a large impact on the drying of the structures. The magnitude of the vapour permeation resistance of the epoxy coating was determined on 10 mm thick specimens taken from the surface of the concrete block. The specimens were collected from 36 concrete cylinders. On half of the specimens, the epoxy coating was ground off with a diamond saw in order to determine the moisture transport properties of the concrete close to the surface. During grinding and preparation, four of the specimens were damaged and were removed.

Eighteen of the 32 test specimens had epoxy coating and 14 were without the coating. Six different climatic conditions were included, in accordance with the specifications listed in Table 6. Three samples were used in each climate, except that in the case of specimens without epoxy at approximately 75 and 85% RH, only two specimens were used. Sixteen specimens were stored in a climate chamber with 55 %RH and 20 °C, and the remainder were placed in an oven at 50 °C. The saturated salt solutions, as presented in Table 5, were used for the different RH values.

Table 6. Test specimens and the corresponding test conditions. The exposure of the specimens was done at different temperatures, 20 °C (1) and 50 °C (2). RH in the cups was established with different saturated salt solutions, as presented in Table 5.

	Core Diameter [mm]	Specimen Thickness [mm]	Specimen Depth [mm]	Temp. [°C] (1)	(2)	RH [%]: Surroundings (1)	(2)	RH [%]: Cup (1)	(2)	No.
Epoxy: Vapour resistance	94	10	0–10	20	50	55	10	75 85 98	74 81 96	32

The measurements were conducted at the Division of Building Materials, Faculty of Engineering, Lund University. Because of the relatively stable moisture content in the air (approximately 4 g m^{-3}) in Lund, Sweden, during winter, the RH was approximately 10 % in the oven during the measurement period. An oven was used, as there was no access to a climate chamber for testing at elevated temperatures. This approach made the comparison at different temperatures more indecisive, as measurements at different RH intervals were compared later.

During the initial exposure of the specimens in the oven, four of the epoxy coated specimens rose from the glass cup as the air expanded in the cup when heated. However, they were pressed back into the right positions when this was observed. One specimen with 75 %RH, two with 81 %RH and one with 96 %RH were affected. No clear evidence of any effect was observed during the prolonged measurements. Only one of the affected specimens (75 %RH) showed the highest moisture flow compared with the others in the same climatic condition. This indicates that the sealing function of the bitumen and Al-tape was not significantly damaged.

The specimens without epoxy coating were capillary saturated before the cups were assembled, to make sure that all the specimens were approaching the steady state of flux through desorption. The specimens with epoxy coating were not treated in the same way because of high vapour permeation resistance in comparison with concrete. It was expected that the epoxy coating would be dominant for the overall vapour resistance. Any effect due to difference in moisture transport coefficients between adsorption and desorption was thereby considered negligible.

In order to properly determine the vapour permeation resistance of the epoxy, the RH directly under the coating must be known. In this study, it was not possible to measure RH because of the setup design. Two alternative methods were chosen to quantify the influence of the epoxy. The first was to consider the epoxy coating and the 10 mm thick concrete layer as a composite. The outer 10 mm in the structure should act in the same manner as the setup; hence, this approach should give the needed information while evaluating the effect.

The composite approach was however not considered valid for evaluating the section of a structure thinner than 10 mm. This was because of the moisture dependency of the coefficient for concrete. At lower RH levels, the influence from the concrete will increase in relation to the influence from the epoxy, as observed in the results from the measurements; this makes the composite dependent on size. If the vapour permeation resistance of the epoxy is assumed to be constant and not RH dependent, an alternative approach was to consider the measured results only in high RH interval. Concrete has a direct moisture dependency that results in significant increase in moisture transport coefficient below approximately 65 %RH and above 90 %RH, as illustrated in Figure 10. If the epoxy coating is assumed to be more resistant to moisture flow than concrete, then the main RH gradient should be over the epoxy coating at steady state. At high RH, the concrete moisture transport coefficient is the highest, and consequently the epoxy coating should be the most dominant and thereby should the obtained results represent the epoxy coating.

The water vapour permeation resistance of the composite, epoxy and concrete, was determined based on the steady state moisture flux measurements. In Figures 11 and 12, the moisture transport coefficients for both temperatures are presented. The specimens is named HAE (Heated, location A, Epoxy), HA (Heated, location A), ANE (Location A, Neutral temp., Epoxy) and AN (location A, Neutral temp.).

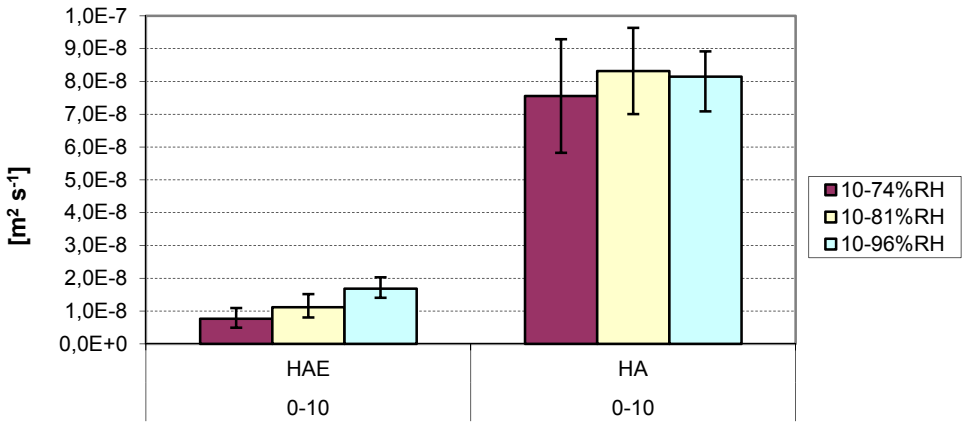

Figure 11. Average moisture transport coefficient measured through cup method on 10 mm thick epoxy-concrete composite HAE and concrete HA, at 50 °C and 10 %RH. The error bars represent the max and min values.

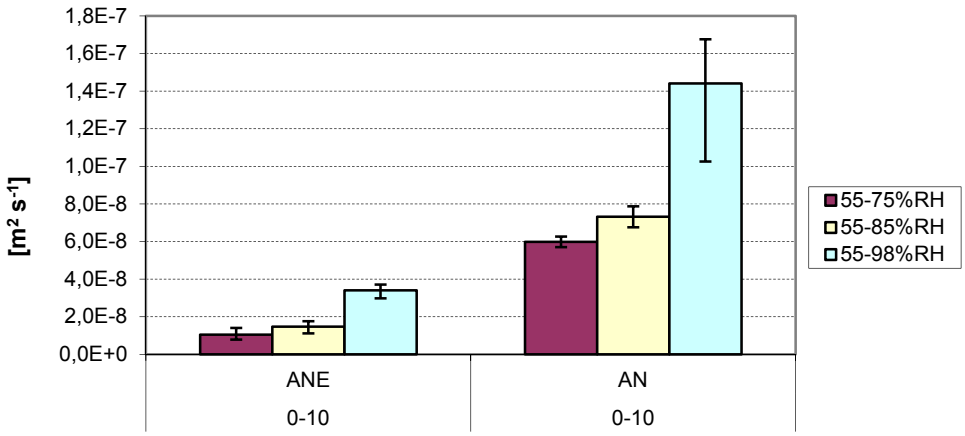

Figure 12. Average moisture transport coefficient measured with cup method on 10 mm thick epoxy-concrete composite ANE and concrete AN, at 20 °C and 55 %RH. The error bars represent the max and min values.

The moisture transport coefficient was further transformed to vapour permeation resistance as given by to Eq. 13.

$$Z = \frac{dx}{\delta_v} \tag{13}$$

where

Z	[s m^{-1}]	Vapour permeation resistance
x	[m]	Coordinates
δ_v	[m^2 s^{-1}]	Moisture transport (v)

The moisture transport coefficient, vapour resistance and an equivalent concrete thickness compared to the surface concrete are presented in Table 7.

Table 7. The moisture transport coefficients of epoxy coated concrete composite samples, recalculations of vapour resistance and an equivalent concrete thickness of the specimens in relation to the concrete samples without epoxy.

50 °C	Moisture transport coefficient, δ_v [m^2 s^{-1}]	Vapour permeation resistance, Z [s m^{-1}]	Equivalent concrete thickness [mm]
10–74 %RH	7.64×10^{-9}	1.30×10^{6}	98
10–81 %RH	1.12×10^{-8}	8.84×10^{5}	74
10–96 %RH	1.68×10^{-8}	5.97×10^{5}	49
20 °C			
55–75 %RH	1.05×10^{-8}	9.70×10^{5}	58
55–85 %RH	1.47×10^{-8}	6.87×10^{5}	50
55–98 %RH	3.40×10^{-8}	3.34×10^{5}	48

The difference in the moisture transport coefficients at the two temperatures can partly be explained by the different RH interval in the setups. The moisture transport coefficient of concrete is strongly moisture dependent, as earlier illustrated in Figure 10, and the concrete may thus have an increased influence on the 50 °C specimens in comparison to those at 20 °C. The low RH at 50 °C was a consequence of exposing the specimens in an oven instead of exposing them in a climate chamber.

No moisture dependency was observed for the moisture transport coefficient of the specimens from the surface that where without epoxy (HA) at 50 °C. The reason was not known, but the measured result may be because of crack formation in the specimens resulting from the increased temperature or specimen preparation. This observation was not further studied in this work. The moisture transport coefficient was however in the same region as in the case of the measurements at 20 °C, which indicates that there were no drastic variations in the material.

Using the model presented in [56] (see Eq. 11) with the measurements gave the moisture transport coefficient in the additional intervals, 75–85 %RH and 85–97 %RH, for the measurements at 20 °C, and 75–81 %RH and 81–96 %RH for the measurements at 50 °C. The results are presented in Figures 13 and 14 together with the measured average values for the measurements at 50 °C and 20 °C, which are presented in Figures 11 and 12.

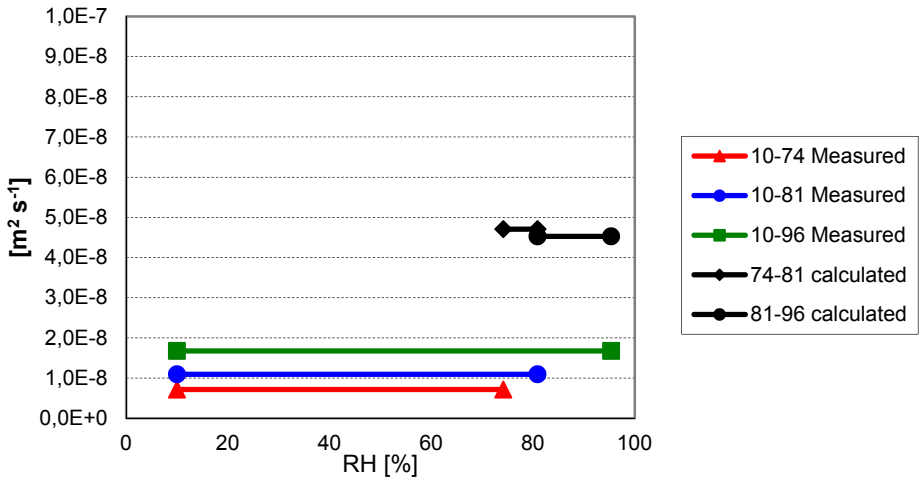

Figure 13. Measured and calculated moisture transport coefficients of epoxy coated specimens HAE at 50 °C. The moisture transport coefficients in the intermediate intervals were determined based on the mean values with measurement errors as presented in Figure 11.

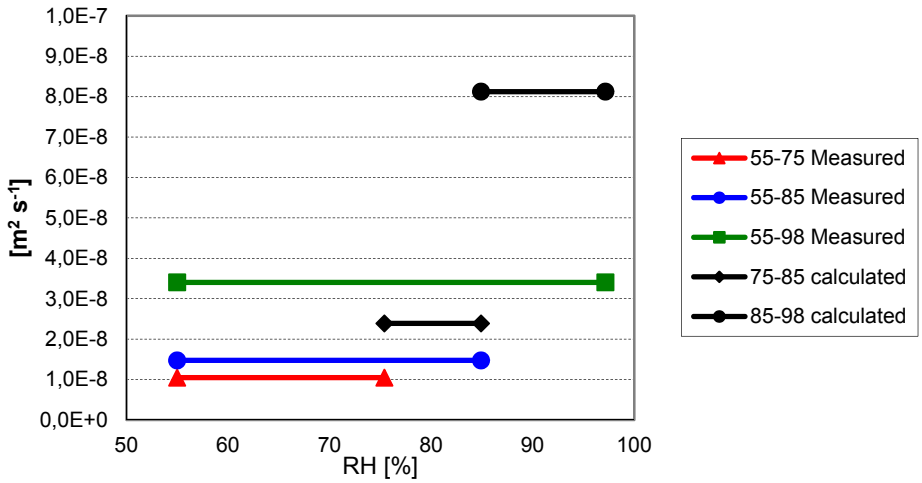

Figure 14. Measured and calculated moisture transport coefficients of epoxy coated specimens ANE at 20 °C. The moisture transport coefficient in the intermediate intervals was determined based on the mean values with measurement errors as presented in Figure 12.

The results show a clear trend that the vapour permeation resistance of the epoxy coating is significantly higher than that of concrete, both at low and high temperatures. The moisture dependency measured might be due to the moisture dependency of the concrete; this may, to some extent, also explain the temperature dependency observed because of the larger RH interval. Another temperature dependent factor can be the potential swelling of the epoxy when heated.

If the epoxy vapour permeation resistance is assumed to be constant and independent of humidity and temperature, the results obtained from the upper RH interval should give a good approximation of the vapour resistance. Based on the results at 20 °C and in the RH interval 85-98 %, the moisture transport coefficient, δ_v, was 8×10^{-8} m² s⁻¹. Redefined, when considering RH as the transport potential, the moisture transport coefficient δ_ϕ was 1.38×10^{-9} kg m⁻¹ s⁻¹ i.e. a vapour permeation resistance Z_ϕ of $7.2\cdot10^{6}$ m² s kg⁻¹. This result was considered when included in the model for moisture transport in the reactor containment concrete for the reactor at Ringhals, as presented in **Paper VI** and summarized in Chapter 6. Other vapour permeation resistances was needed for the Forsmark plants in the model, in order to validate the model to the in-situ measurements.

4.2.2 Moisture transport coefficient

The moisture transport coefficients of different concrete compositions have earlier been described by researchers, e.g. Hedenblad [52]. Based on his measurements, a function (Eq. 12) was designed. The function was however valid only for concrete with a w/c-ratio of 0.4. However, if the moisture transport coefficient in the lower RH interval for a concrete composition is known, and if the internal relation of the transport coefficient's dependency on moisture is assumed to be the same as for the measurements by Hedenblad, than should the basis of Eq. 12 also be valid for similar concretes. Through these assumptions it should be possible to adapt the moisture transport coefficient function, as given in Eq. 12, and based on the new measurements of the moisture transport coefficient at low RH, get a fairly good approximation of the moisture transport coefficient in the entire RH interval for a new concrete composition. The approximation would however not consider that a more dense concrete would reduce moisture transport coefficient more in the higher RH interval than in the lower RH interval, as of the larger reduction of permeability than diffusivity with a denser material.

Twenty-one concrete cylinders from the inner containment wall at Ringhals 4 were used to determine the moisture transport coefficient. Three specimens, 20 mm thick discs, were taken from each of the cylinders. The discs were taken from 40–60 mm (B), 100–120 mm (C) and 240–260 mm (D) depths. All the specimens were capillary saturated and their envelope surface was sealed with a heated bitumen strip in the same manner as for the epoxy coated specimens, as described in *Section* 4.2.1.

The moisture flow measurements were done on 63 specimens. The test series included seven climatic conditions. Thirty-six specimens were placed in a climate chamber at 20 °C

and 55 %RH and 27 specimens were placed in an oven at 50 °C. The measurements were conducted at the Division of Building Materials, Faculty of Engineering, Lund University. Because of the relatively stable moisture content (approximately 4 g m^{-3}) in the air in Lund, Sweden, during winter, the RH in the oven was approximately 10 % during the measuring period. An oven was used, as there was no access to a climate chamber for testing at elevated temperatures. This approach made the comparison between the different temperatures more indecisive, as different RH intervals were compared later. Three specimens from each depth were studied in both the climate chamber and in the oven. The seven different steady state climatic conditions are presented in Table 8, together with the specimen specifications.

Table 8. Different setups for moisture flow measurements. A total of seven different steady state climatic conditions were included, four at 20 °C (1) and three at 50 °C (2).

	Specimen Diameter [mm]	Specimen Thickness [mm]	Specimen Depth [mm]	Temp. [°C] (1)	Temp. [°C] (2)	RH [%]: Surrounding (1)	RH [%]: Surrounding (2)	RH [%]: Cup (1)	RH [%]: Cup (2)	No.
Moisture transport coefficient	94	20	40–60 100–120 230–250	20	50	55	10	33 75 85 98	- 74 81 96	63

The specimens were capillary saturated to ensure that they were under desorption during the entire measuring phase. Variations in the moisture transport coefficients between adsorption or desorption have been found in earlier studies, e.g. [53]. If only the moisture transport coefficient for desorption is considered, the total accuracy reduces when used on a dynamic moisture model. However, it was assumed that the concrete within the reactor containment is primarily exposed for drying, and will be in this state for a prolonged period of time. Surface variations may occur, but they were not considered in this study.

All specimens used in the study were 20 mm thick, which was thinner than a representative test specimen traditionally considered for concrete specimens, i.e. the minimum section size should be greater than three times the largest particle size, which corresponds to 96 mm for the concrete at Ringhals 4. The smaller thickness was chosen, even though it does not fulfil the representative size of the specimen thickness, and carries the potential risk of throughout aggregates. Throughout aggregates was believed to be the main error source when thinner specimens are used. Specimens with throughout aggregates may have a higher total moisture flow owing to higher porosity in the interface zone between the aggregates and the cement paste. These interface zones are normally referred to as the interfacial transition zone (ITZ) [57]. The approach in this work was to study the changes over the depth of the structure, and it was believed that the size effect would be small. In addition, the approach with thinner specimens was chosen partly based on the observations earlier presented by Hedenblad [52] that thick specimens may need a couple of years before steady state moisture flow occurs.

There have been no studies so far regarding the influence on moisture flow due to ITZ on throughout aggregates. To identify any potential ITZ influences from large aggregates, all specimens were inspected and throughout aggregates were identified; their images were captured prior to the assembly of the cups. When the moisture flow had reached the steady state condition, the specimens that had moisture flux deviating significantly from the average were inspected to determine whether any aggregates interpenetrated the specimen. No such correlation was found.

All the potential errors from the usage of thinner specimens were not evaluated in this study. Further studies are needed to check whether a sample thickness of at least three times the largest aggregate is crucial to determine the moisture transport coefficient for concrete. The potential consequence of the choices made in this study was that the moisture resistance is underestimated and that the transport coefficient is somewhat lower, as the thinner specimens may lead to a shorter average water molecule transport length, thus giving a smaller transport resistance. The average results from the measurements should however give a fairly good estimation of the coefficient of the Ringhals 4 concrete.

The surface area of the specimens was also in the lower band of acceptable size. With the maximum aggregate size of 32 mm, the surface area of the specimens should not be smaller than 96×96 mm². Having the representative surface area permits the measurements to convert the flow [kg s^{-1}] into flux [kg m^{-2} s^{-1}] with a reasonably small uncertainty. However, if the combined surface of several specimens was considered, the assumption of representative size is still valid. However, using several smaller specimens increases the scatter of the results, as there may be a notable variation in the cement paste to aggregate ratio between the specimens.

The moisture transport coefficient determined on specimens with different thicknesses, as presented by Hedenblad [52], showed a clear correlation that a thicker specimen corresponded to a higher moisture transport coefficient; similar findings has been reported earlier also. All the specimens in the comparison had thickness of at least three times the largest aggregate size. In the measurements conducted by Hedenblad, it seemed that the size effect was larger at high w/c-ratios; this was however not discussed in the thesis. One plausible explanation for the difference, according to Hedenblad, was that moisture transport in concrete is in fact non-Fickian. This hypothesis was however not tested or considered in this study.

Figures 15 and 16 present the moisture transport coefficients of the concrete specimens from the different depths and for the two different temperatures. As a comparison, the moisture transport coefficients of the plain concrete specimens, HA and AN, from the epoxy coating measurements in *Section* 6.2.1, are also included.

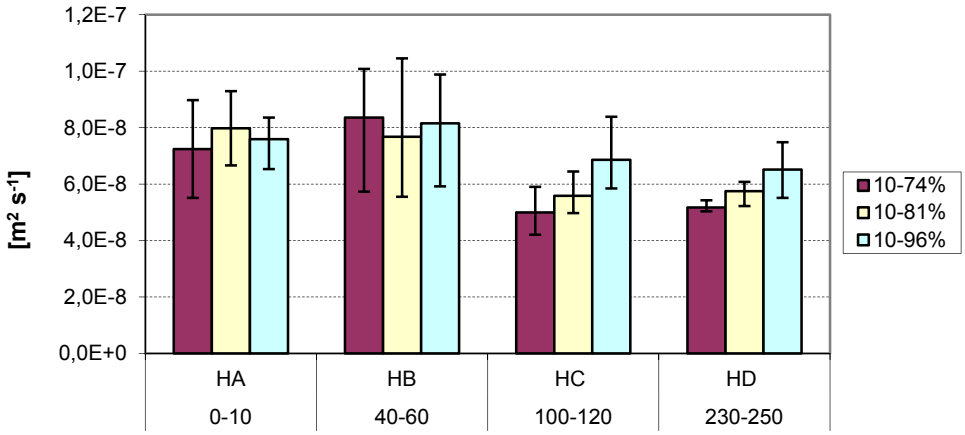

Figure 15. Average moisture transport coefficient from cup method evaluation on 20 mm thick concrete specimens, HB, HC, and HD. Moisture flux was determined at three different depths at 50 °C and with 10 %RH. HA corresponds to the results of the outer 10 mm thick specimen presented earlier in *Section* 4.2.1. The error bars represent max and min values.

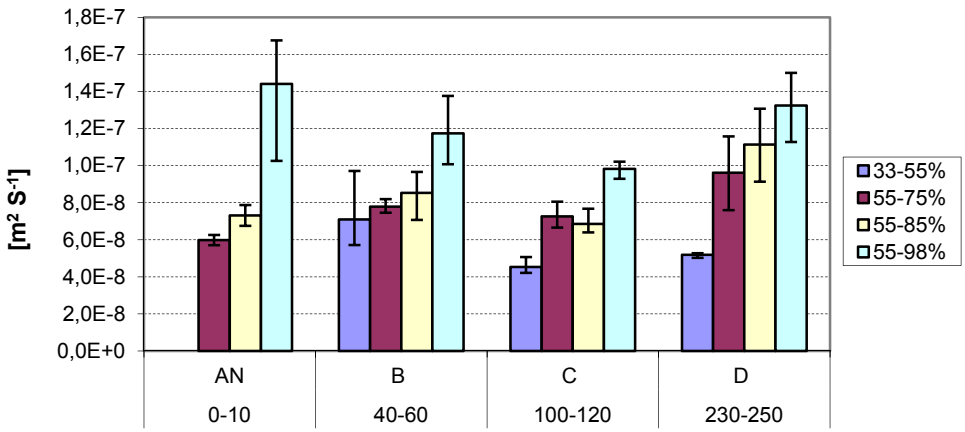

Figure 16. Average moisture transport coefficient from cup method evaluation on 20 mm thick concrete specimens, B, C and D. Moisture flux was determined at three different depths at 20 °C and with 55 %RH. The specimens AN corresponds to the results of the outer 10mm thick specimens presented earlier in *Section* 4.2.1. The error bars represent max and min values.

The measurements at 20 °C show that there were no significant variations with depth in the concrete cylinders. There was however a large scatter in the measurements, both between different depths and in different conditions. However, the measurements indicated the expected moisture dependency. The measurements on specimens close to the surface that was exposed to 50 °C (HB) were not considered accurate. The large scatter within each RH

range and the lack of moisture dependency implied that the specimen might have been damaged during the heating. The same tendency was also observed on the 10 mm specimens HA. Because of this reason, the results from HA and HB were not considered further.

The model described in [56] and given by Eq. 11 was applied to the results. Figures 17–21 present the average moisture transport coefficient from the measurement series B, C, D, HC and HD, with the measurement errors presented as max and min values given in Figures 15 and 16, and the results from the Anderberg and Wadsö model. The moisture transport coefficients from the overlapping intervals, determined from Eq. 11, were done only on the mean values in each RH span.

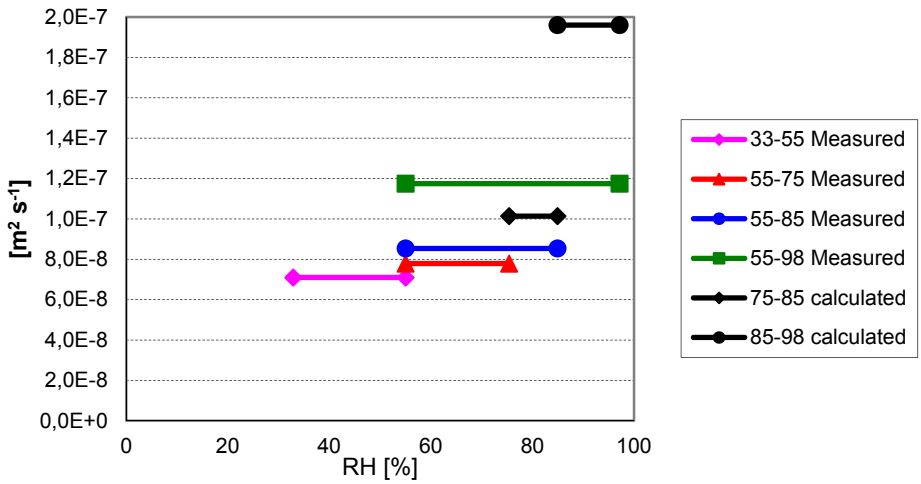

Figure 17. B specimens: Average moisture transport coefficient of concrete specimens from 40–60 mm depth at 20 °C. The moisture transport coefficient in the overlapping spans was determined based on the mean values.

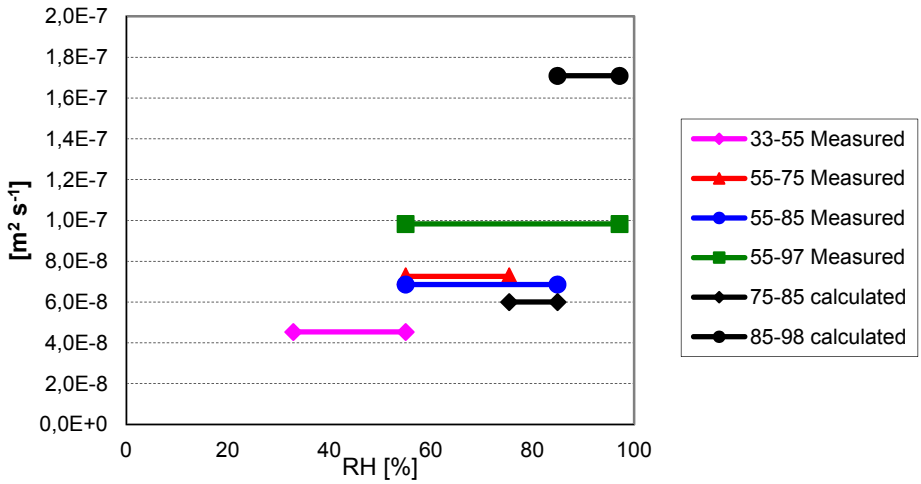

Figure 18. C specimens: Average moisture transport coefficient of concrete specimens from 100–120 mm depth at 20 °C. The moisture transport coefficient in the overlapping spans was determined based on the mean values.

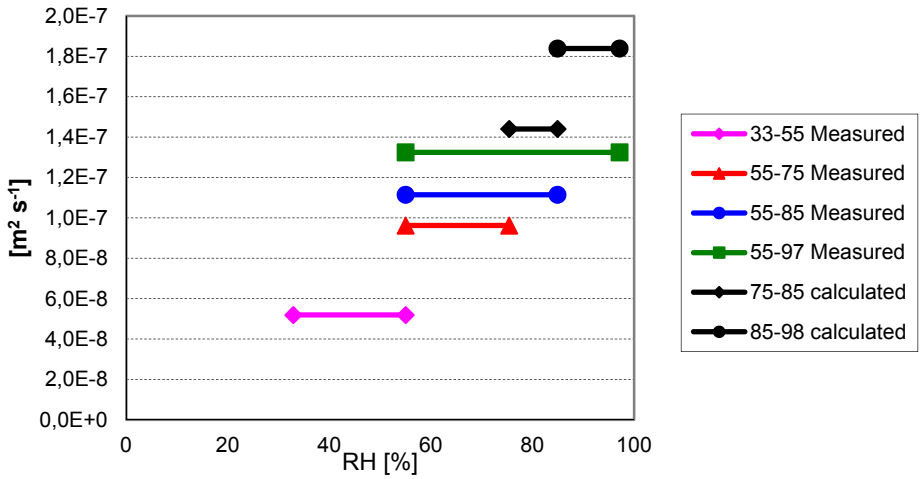

Figure 19. D specimens: Moisture transport coefficient of concrete specimens from 230–250 mm depth at 20 °C. The moisture transport coefficient in the overlapping spans was determined based on the mean values.

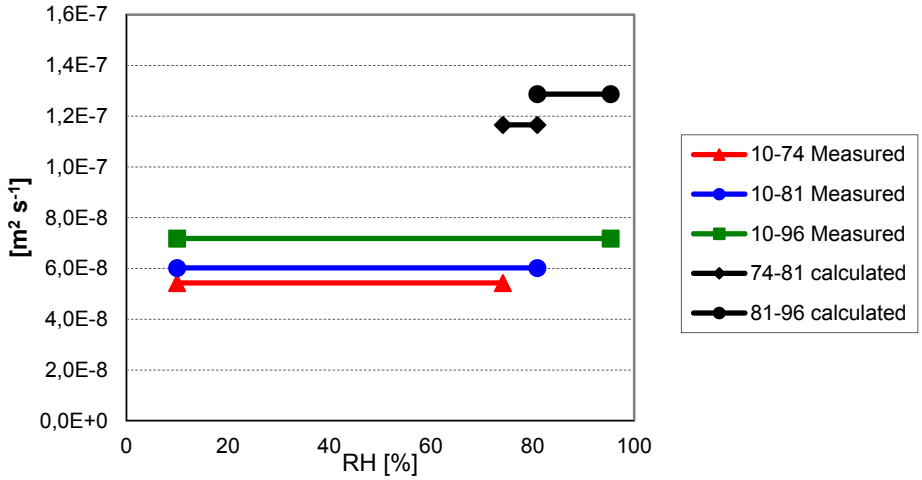

Figure 20. HC specimens: Moisture transport coefficient of concrete specimens from 100–120 mm depth at 50 °C. The moisture transport coefficient in the overlapping spans was determined based on the mean values.

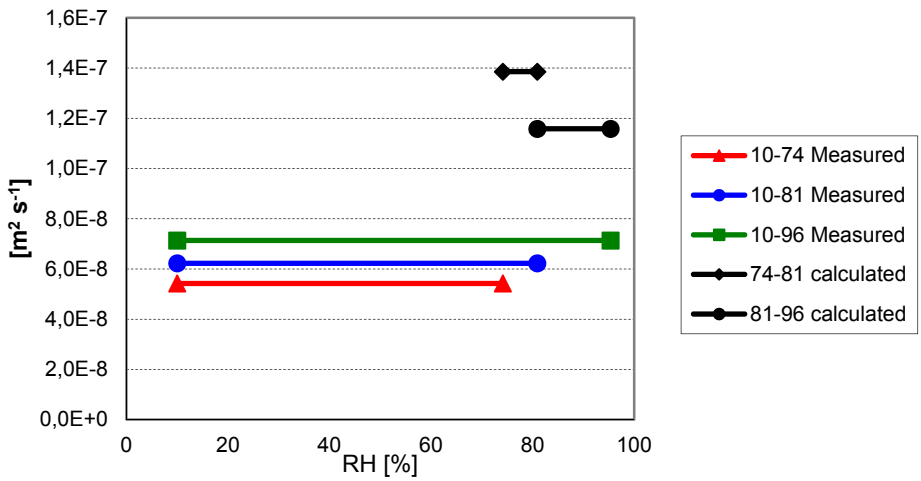

Figure 21. HD specimens: Moisture transport coefficient of concrete specimens from 230–250 mm depth at 50 °C. The moisture transport coefficient in the overlapping spans was only determined based on the mean values.

As for the measurements on the epoxy coated specimens, the values of some of the coefficients were considered as unlikely. This was especially the case for the moisture transport coefficient determined on the HD specimens in the interval 74–94 %RH, shown in Figure 21. However, it was not possible to determine the reason for the higher moisture transport coefficient in the RH interval 74–81 %RH compared with the results from the RH interval 81–96 %RH.

The results showed that the moisture transport coefficient was significantly lower than that obtained by Hedenblad [52]. The average moisture transport coefficient in the low RH intervals, based on the values in all specimens, was approximately 0.56×10^{-7} m² s⁻¹ at 20 °C. The corresponding moisture transport coefficient measured by Hedenblad [52] on a similar concrete with w/c-ratio of 0.40, but 100 mm thick, was 1.3×10^{-7} m² s⁻¹. The concrete at Ringhals 4 thus had a moisture transport coefficient that was between 1/2 and 1/3 of that measured by Hedenblad. The difference is possibly on account of a higher degree of hydration, and therefore the concrete had a more dense cement paste.

Assuming that the function, as given in Eq. 12, *Section* 4.2, describing the moisture transport coefficient for the concrete with a w/c-ratio of 0.4, was valid for other similar concrete composition, if adapted with regard to the coefficient at low RH, the R4 concrete samples could be expressed by Eq. 14. Figure 22 shows a comparison of the results of the material study at 20 °C, shown in Figures 17–19, when presented as the mean values in each RH interval, obtained using Eq. 14. A good correlation was observed, which indicates that the earlier assumption is valid for this concrete composition. This function, Eq. 14, was later used in **Paper VI** for moisture transport calculations.

$$\delta_v = 0.5606 \times 10^{-7} \cdot e^{2.455 \cdot \phi^{5.35}} \tag{14}$$

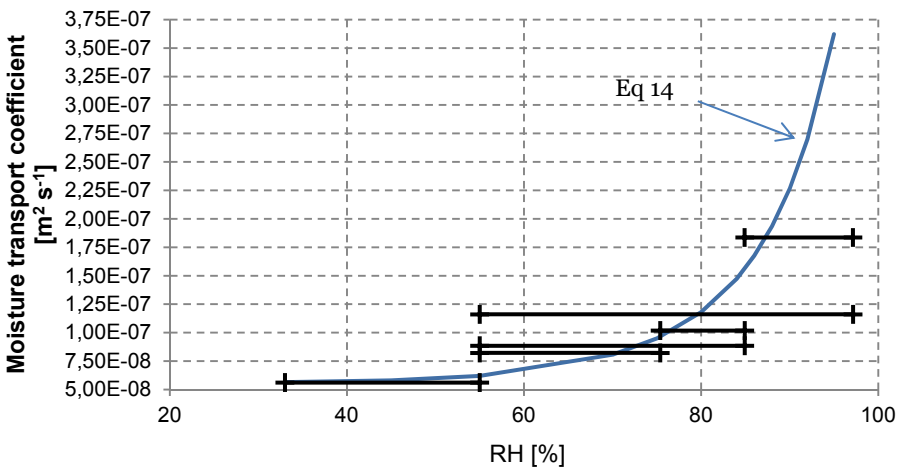

Figure 22. Average measured moisture transport coefficient, at 20 °C, for the Ringhals 4 concrete specimens. The average values were based on the B, C and D measurements, shown in Figure 16. The blue lines correspond to the simulated results using Eq. 14.

4.3 Variation in degree of hydration

The hydration process of cement is not linear, and the larger part of hydration occurs within the first few days and weeks. The speed of the hydration decreases rapidly with time and the concrete may still not have reached full hydration after several years. The variations depend mainly on w/c-ratio, curing conditions, access to water and the cement type. The hydration process stops either because of absence of space or water, i.e. when the RH decreases below about 85 % [58]. The space available for the hydration products reduces with decreasing w/c-ratio. The theoretical minimum w/c-ratio that can achieve full hydration is 0.42, assuming that there is no access to external water [59]. With external water access, the limit is 0.36 [59], and if unlimited space is assumed, the limit is 0.25; this is the amount of chemically bound water required for fully hydrated cement.

Variations in the degree of hydration in a structure can arise because of sustained temperature gradients or early drying of the surface. A variation in hydration would lead to variations in material properties such as the moisture transport coefficient.

The main cement clinker components, which are the reactive particles that together with gypsum make the ordinary Portland cement, are the following.

- C_3S Alite Tricalcium Silicate
- C_2S Belite Dicalcium Silicate
- C_3A Celite Tricalcium Aluminate
- C_4AF Ferrite Tetracalcium Aluminioferrite

When water is added to the dry concrete mixture, a reaction starts between the cement and water, i.e. the cement starts to hydrate. Water reacts with the different clinker components and cement gel is formed. The main hydration products in the cement gel are calcium hydroxide (CH), calcium silicate hydrate (C-S-H), Ettringite (AFt) and monosulphate (AFm). The C-S-H is the main product and represents a group of crystalline formations which is considered as poorly crystallized and partly amorphous, and hence normally referred to as C-S-H gel [60].

During the hydration of cement, the mixing water is physically and chemically bound in the cement gel. With the model developed by Powers and Brownyard [58, 59], the amount of bound water can be determined for a specific concrete if the clinker composition and the degree of hydration are known. Normally, it is assumed that the fully hydrated cement chemically binds water corresponding to approximately 25 % of the cement dry mass. However, this value varies depending on the clinker composition of the specific cement.

The results from Power's and Brownyard's work have been used in several studies to determine the degree of hydration or to estimate the amount of different components, e.g. [61-63]. A traditional way to determine the degree of hydration is through loss on ignition (LOI) measurements. The LOI method is based on the assumption that all the water in hydrated cement is extracted if the material is exposed to 1050 °C until mass equilibrium is

reached. If all the evaporable water is assumed to be extracted when exposed to 105 °C, the mass loss between 105 °C and 1050 °C corresponds to the non-evaporable water i.e. water bound in the hydrated cement. By comparing this value with the theoretical maximum bound water, the degree of hydration can be determined.

One weakness of the LOI method is that it is hard to identify and quantify the potential influence of aggregates or other components. For instance, aggregates that contain components such as $CaCO_3$, limestone, or carbonated cement will lose mass during the LOI test because of decarbonisation. If the amount of a component, e.g. limestone, is not known, a proper determination cannot be made.

When exposed to elevated temperature the cement hydration products are decomposed. Dividing the decomposition into different steps in which different components lose their water and decompose gives an overview of the process. One way to describe the decomposition is to divide it into three intervals [64].

- 105 °C to 440 °C: Dehydration of mainly C-S-H gel, AFt, etc.
- 440 °C to 580 °C: Dehydroxylation of CH
- 580 °C to approximately 1000 °C: Decarbonation of CaCo3

The temperature interval for dehydroxylation may vary somewhat between different studies, but the decomposition of CH at approximately 450 °C is well documented [61, 62, 64-66].

As an alternative to the LOI method, the mass change in the different intervals can be evaluated separately, e.g. the dehydroxylation of CH. While performing a thermogravimetric analysis (TGA), the temperature is plotted against the mass loss. The dehydroxylation can clearly be seen as an increased mass loss at approximately 450 °C during the TGA of cement paste or concrete. The dehydroxylation can also be identified when a differential thermal analysis (DTA) or differential scanning calorimetry (DSC) is performed. With both techniques, it is possible to determine whether there is an endothermic or exothermic reaction at different temperature intervals. Decomposition of CH, which is an endothermic reaction [61], shows as a peak in the DTA or DSC measurements.

Using the knowledge from Powers and Brownyard, together with TGA, DTA or DSC measurements, it is possible to determine the amount of CH that a specific concrete should contain. This is done through recalculations of the mass loss in the dehydroxylation interval. The recalculation is made based on the hydration reactions for the four main clinker compositions.

Based on a simplified description of the cement clinker reactions, where Afwillite ($C_3S_2H_3$) is the only C-S-H mineral, it is possible to derive CH formation at full hydration in relation to the cement content [kg(CH) kg(cement)$^{-1}$], as given in Eq. 15. The actual cement clinker hydration is more complicated than this generalisation, and is not fully explained by this

estimation. However, this estimation would give an indication of the CH amount or at least it is possible to compare variations over the depth of a structure.

$$CH = \frac{C_3S}{100} \times 0.49 + \frac{C_2S}{100} \times 0.21 - \frac{C_4AF}{100} \times 0.31 \quad (15)$$

By inserting the clinker composition as presented in Table 3, *Section* 4.1, the total CH formation possible in the concrete is 0.234 kg (CH) kg^{-1} (Cement). The dehydroxation the CH decomposition can further be written as follows.

$$Ca(OH)_2 \rightarrow CaO + H_2O$$

The molar mass of CH is 74.093 g mol^{-1}, that of CaO is 56.077 g mol^{-1}, and that of water 18.015 g mol^{-1}. This gives a water to CH ratio of 18.015/74.093 = 0.243. By measuring the amount of water released during the dehydroxation of CH in a cement paste, it is possible to determine the amount of CH that it represents. The quotient between the theoretical CH formation, as given in Eq. 15, and the amount from the TGA measurements gives an approximate degree of hydration based on a smaller temperature interval than LOI. With this approach, the effect from unknown components, e.g. lime stone, is limited; however, carbonation has to be considered.

4.3.1 Measurements and results

The measurements of the amount of CH were made on nine test specimens. The specimens were taken from three depths, 40–50, 150–160 and 250–260 mm and sawed out from three concrete cylinders. All the specimens were then placed in an oven at 105 °C for approximately four hours. The specimens were to be left in the oven until steady state to remove all evaporable water. However, because of the tight time schedule, this was not possible. The mass loss close to 450 °C, which was the focus in these measurements, should however not be influenced by this change. The dry mass of the sample was used to determine the cement content of each specimen, and hence a systematic error was inserted. This error should be the same for all samples.

After the specimens had been stored in the oven, the specimen was crushed with a hammer and ground in a mill, down to a size of approximately 200 μm. The powder from each specimen was placed in a diffusion tight plastic cup to limit further carbonation. Carbonation of hydrated cement, where CH transforms to $CaCO_3$, requires access to CO_2, as well as some moisture for the process to proceed. One approach to reduce the carbonation rate, apart from limiting the CO_2 exposure, is to dry the sample. The carbonation rate decreases with respect to the highest rates for both high and low RH. A high RH results in slow CO_2 ingress, and a low RH reduces the moisture needed for the reaction. The RH in the ground sample was unfortunately not known. The period after grinding was thereby the most crucial with regard to carbonation because of the much larger surface area of the powder than of the concrete specimens. However, because all

specimens were treated in the same manner, the potential carbonation would be fairly equal between all samples, and consequently, this would not result in a faulty result for an internal comparison.

Approximately 2 g from each cup was placed in a TGA, LECO TGA 500. The measurements were done at Cementa Research in Slite, Sweden. One additional TG/DSC measurement was made with Netzsch STA 449 C w. The sample was approximately 40 mg and the TG and DSC measurements were made to verify that the endothermic peak that appears during the dehydroxation of CH corresponds to the results from the TGA measurements (see Figure 23). The location of the endothermic peak in the temperature interval 440 to 500 °C corresponds to the big drop of mass observed in the TG measurements and was due to the dehydroxylation of CH. The second peak, close to 570 °C, was due to α-δ transformation of quartz in the aggregates [67]

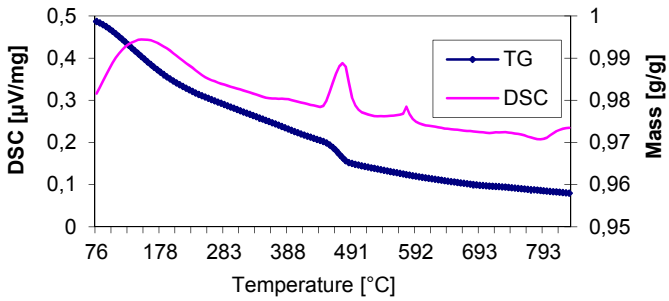

Figure 23. Measurements of TG and DSC of one sample from the inner containment wall at Ringhals 4. The left Y-axis shows the DSC results and the right shows the mass as a percentage of the initial mass of the sample.

The cement content of the specimens used for the TGA was determined by quantifying the amount of CaO in the samples through titration; any effects from CaO that could be present in the aggregates was not considered. However, large quantities of limestone were not likely for this specific concrete because of the geographic location of Ringhals. The cement content was measured on three samples from each plastic cup. The average value was then used to calculate the mass loss of water in relation to the amount of cement in the specimen. This was done in order to eliminate the variation of the aggregate to cement ratio between the samples.

Figure 24 presents the mass loss from 370 °C to 470 °C, in relation to the cement content, of all the nine specimens that were tested in the TGA. The cement content was estimated based on the mass of the sample obtained from the measurements at 105 °C. Instead of considering the entire temperature span, only the main drop close to 440 °C was evaluated. The measured values of mass one temperature step before and one after the above drop, were used for all the nine specimens.

The main purpose of these measurements was to evaluate the potential variations over the structure, and therefore the actual CH amount or degree of hydration was not the primary

objective. The total dehydroxation of CH occurs in a larger interval, and not as a sudden drop. However, by only including the smaller and more direct interval, the influence of other decompositions would be minimized. The accuracy of evaluation of the variation should increase with this assumption. Hence, the external effects should be minimized. The new method was assumed to give a more distinct comparison.

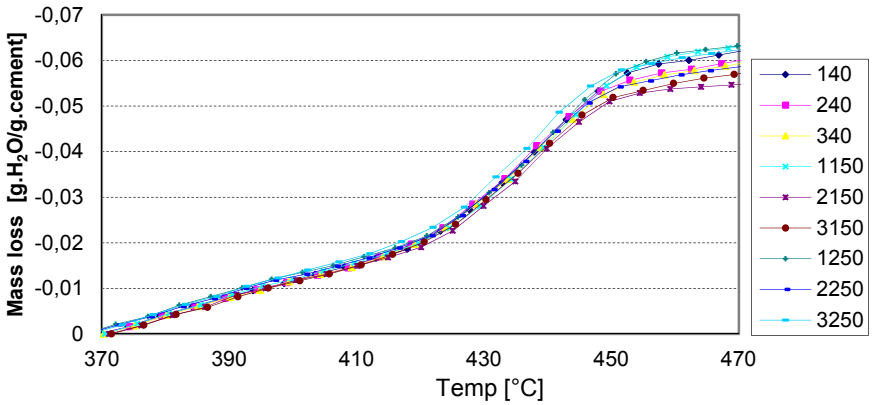

Figure 24. TGA measurement results of nine concrete samples from Ringhals 4. Three samples were taken from each depth and the mass loss is in relation to the cement content of the sample mass at 105 °C.

In Figure 25, the average variation of hydration is plotted based on the relation between amount of theoretical maximum CH and the amount based on recalculation of mass loss when heated. The error bars in Figure 24 correspond to the max and min values.

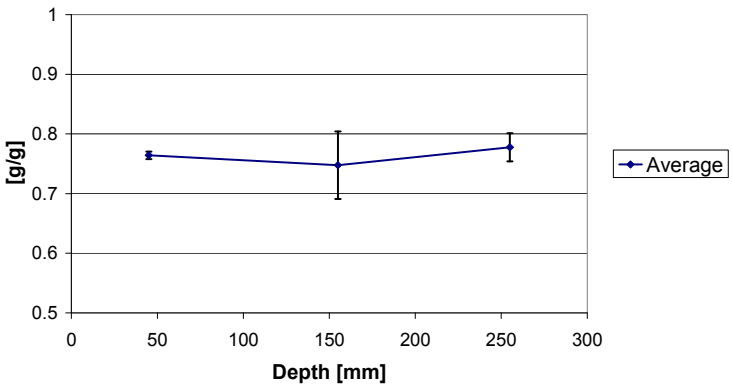

Figure 25. Variations in degree of hydration presented as the approximate amount of CH in relation to theoretical CH max when fully hydrated. The error bars represent the max and min values.

The results presented in Figure 25 show no clear trend of the variation in hydration over the depth of the inner containment wall at Ringhals 4. The assumption that all the CH was decomposed in the measured interval gave a degree of hydration of approximately 75 %. This value is lower than what can be expected on a 30-year old structure. The main reason is that CH decomposes over a larger temperature interval. According to [60], 98 % of the CH is decomposed in the temperature interval 370–580 °C.

The results of the degree of hydration, together with the moisture transport coefficient variations, as presented in *Section* 4.2.2, showed that there was no significant variation over the depth of the structure, and therefore the same models, for e.g. moisture transport coefficient and moisture fixation, can be used for the total depth of each structure. This assumption was used in the model presented in **Paper VI**.

5 Monitoring campaigns

The actual conditions within the reactor containments and the concrete structures in different; reactor types, containment designs and geographic locations were evaluated in order to determine the variations and similarities. A measurement setup for monitoring the moisture and temperature in concrete, in situ and over a prolonged period of time, was thus designed and evaluated. Four monitoring campaigns were conducted to study the climatic conditions inside the nuclear reactor containments during operation. The reactors were chosen to represent four of the five reactor groups described in *Section* 2.1.

The conditions both in the concrete structures as well as the ambient conditions were monitored during one operational year. Four reactors were included in the study: Ringhals 1, Ringhals 4 and Forsmark 2 were monitored during the operational year 2012–2013, and Forsmark 3 was monitored during the year 2013–2014.

The equipment used for accuracy evaluation and monitoring campaigns consisted of RH and temperature measurement probes, HMP 110, from Vaisala OY. The probe measures RH with a Vaisala HUMICAP® 180R sensor, and measures temperature with Pt1000 RTD, 1/3 Class B IEC 751. The data were primary collected with a logger CR1000 and multiplexer AM25T from Campbell Scientific Inc.

The setup, shown in Figure 26, was designed and tested both during accuracy evaluation and in situ monitoring campaigns. The design of the setup is presented and evaluated in **Papers III, IV** and **V**. The evaluation of the measurement setup was done with regard to the following.

- Measurement stability: In situ measurements – **Papers III** and **IV**
- Measurement stability: Laboratory conditions – **Papers IV** and **V**
- Leak tightness of measuring setup – **Paper V**
- Temperature measurement accuracy – **Paper V**
- Equipment environmental sensibility – **Paper V**

Based on the evaluation of the setup, it was concluded that the setup was suitable for long-term measurements. Additional attention is however needed while measuring in shallow depths, as of the increased risk of leakage. It was further concluded that the setup was stable over time if properly installed; however, measurements should not be done for more than one year, as re-calibration of the RH/T probes is advised once in a year. The largest error source identified in the study was temperature misread, especially while measuring in shallow depths. In a non-isothermal condition, additional temperature measurements, e.g.

surface temperature, are suggested, as an accurate temperature gradient is necessary to properly evaluate the moisture distribution.

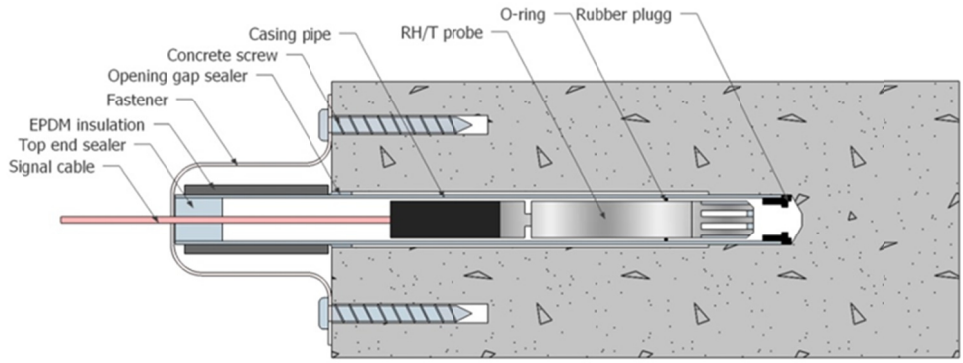

Figure 26. Schematic illustration of the measurement setup and its components

The results from the in situ monitoring campaigns were first presented as preliminary results, and the evaluation of the setup was presented in **Papers III** and **IV**. The external effects on the climatic conditions were evaluated and presented in **Paper II**. The final results from the containment walls at the BWRs, considering the results presented in **Paper V,** are presented in **Paper VI**. In *Sections* 5.1–5.4, the monitoring campaigns are briefly presented together with the measured results from all the zones and all the NPPs included in this study.

5.1 Measurements at Ringhals 1

In Table 9, the positions of the measurement zones are presented. Figure 27 presents a section of the containment with the vertical locations of the zones, and the results are presented in Figure 28.

Table 9. Horizontal and vertical positions of each zone at Ringhals 1, four primary (P) and two secondary (S) measurements. The steam pipes were located at 0° in the upper drywell and the personnel sluice at 90°. The +height 100 corresponds to sea level.

Zone	Depth [mm]	+ Heights [m]	Distance from centre [m]	Angle [°]
1P	Air: 20: 50: 150: 250	112	11.0	120
2P	Air: 20: 50: 150: 250	103	11.0	195
3P	20: 50: 150: 400	103	10.0	195
4P	Air: 20: 50: 150: 400	96	5.8	40
S1	Air: 50: 150	115	11.0	240
S2	Air: 50: 150	106	11.0	30

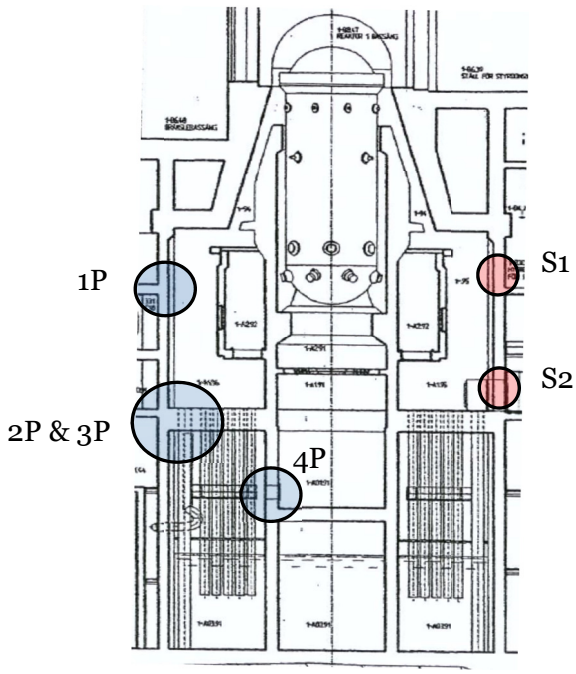

Figure 27. Section of Ringhals 1 with a schematic location of measurement zones. Zones 1P, 2P, S1, and S2 were located in the inner containment wall. Zone 3P was located in the intermediate floor and zone 4P in the wall separating the drywell and wetwell.

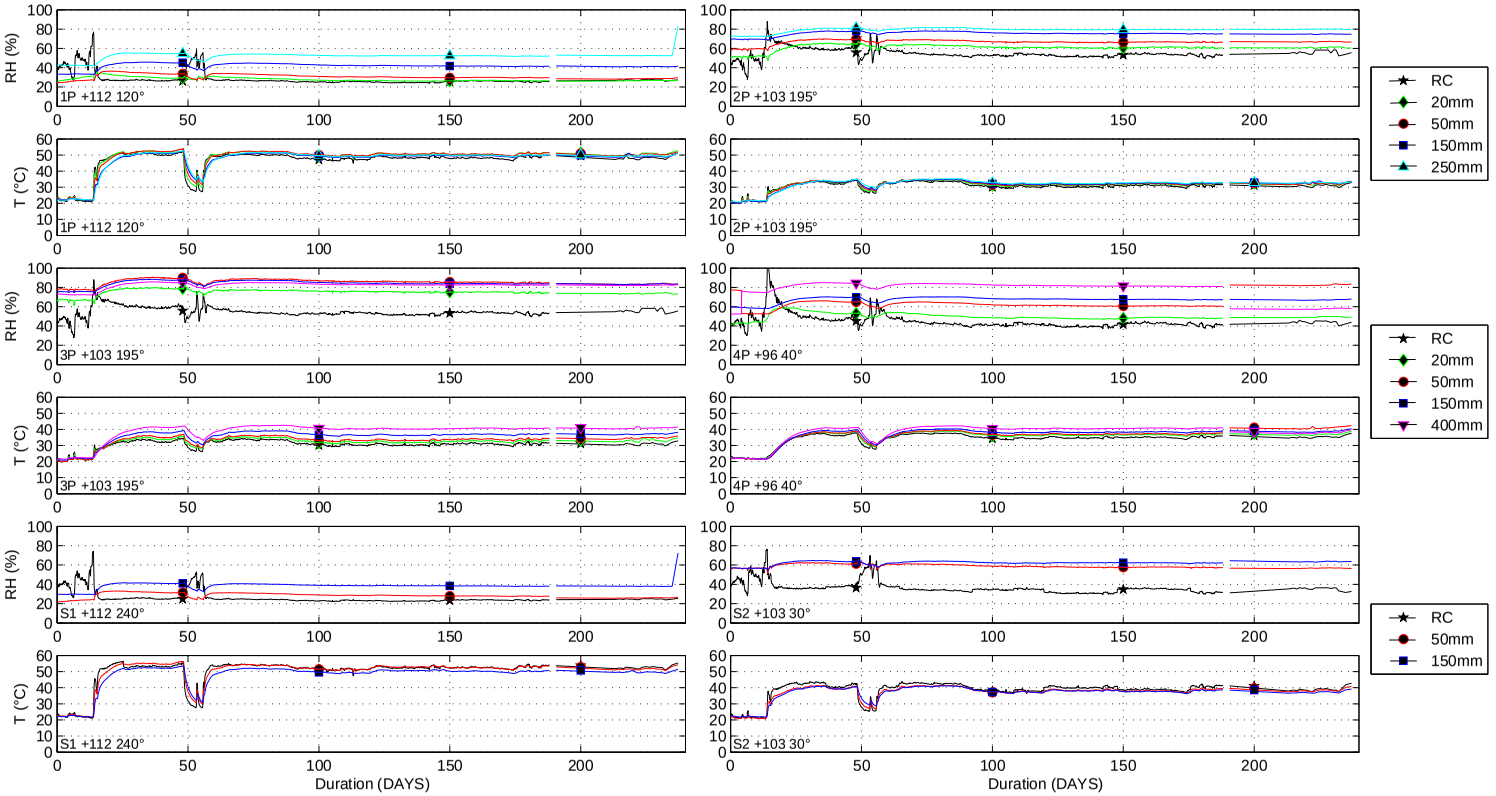

Figure 28. Measured results without adjustments, as described in **Paper V**, from the monitoring campaign in the RC at Ringhals 1. The measurements on Ringhals 1 started in June 2012 and were conducted until January 2013. Measurements were done in six zones in accordance with the details in Figure 27 and Table 9. The measurements were stopped prematurely because of setup failure.

5.2 Measurements at Forsmark 2

In Table 10, the positions of the zones are presented, and Figure 29 shows a section of the containment where the position in terms of the height of the zones is illustrated. The measured results during one operational year are presented in Figures 30 and 31.

Table 10. Horizontal and vertical position of each zone at Forsmark 2, four primary (P) and two secondary (S) measurements. The steam pipes were located at 0° in the upper drywell and the personnel sluice at 90°. The +height 100 corresponds to sea level.

Zone	Depth [mm]	+ Heights [m]	Distance from centre [m]	Angle [°]
1P	Air: 20: 50: 120: 190	131	11.0	270
2P	Air: 20: 50: 120: 190	124.5	11.0	60
3P	Air: 20: 50: 120: 250	114	5.2	260
4P	Air: 20: 50: 120	102	5.2	10
S1	Air: 50: 120	131	11.0	110
S2	Air: 50: 120	124.5	11.0	190

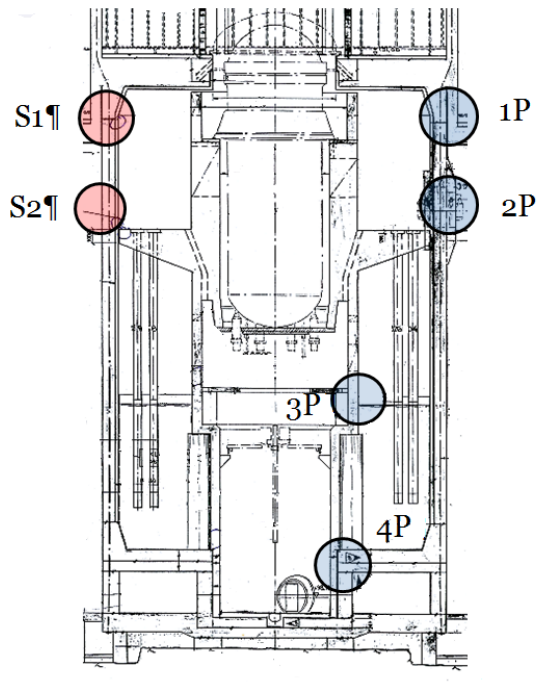

Figure 29. Section of Forsmark 2 with a schematic location of measurement zones. Zones 1P, 2P, S1, and S2 were located in the inner containment wall, and zones 3P and 4P in the wall separating the lower drywell and wetwell.

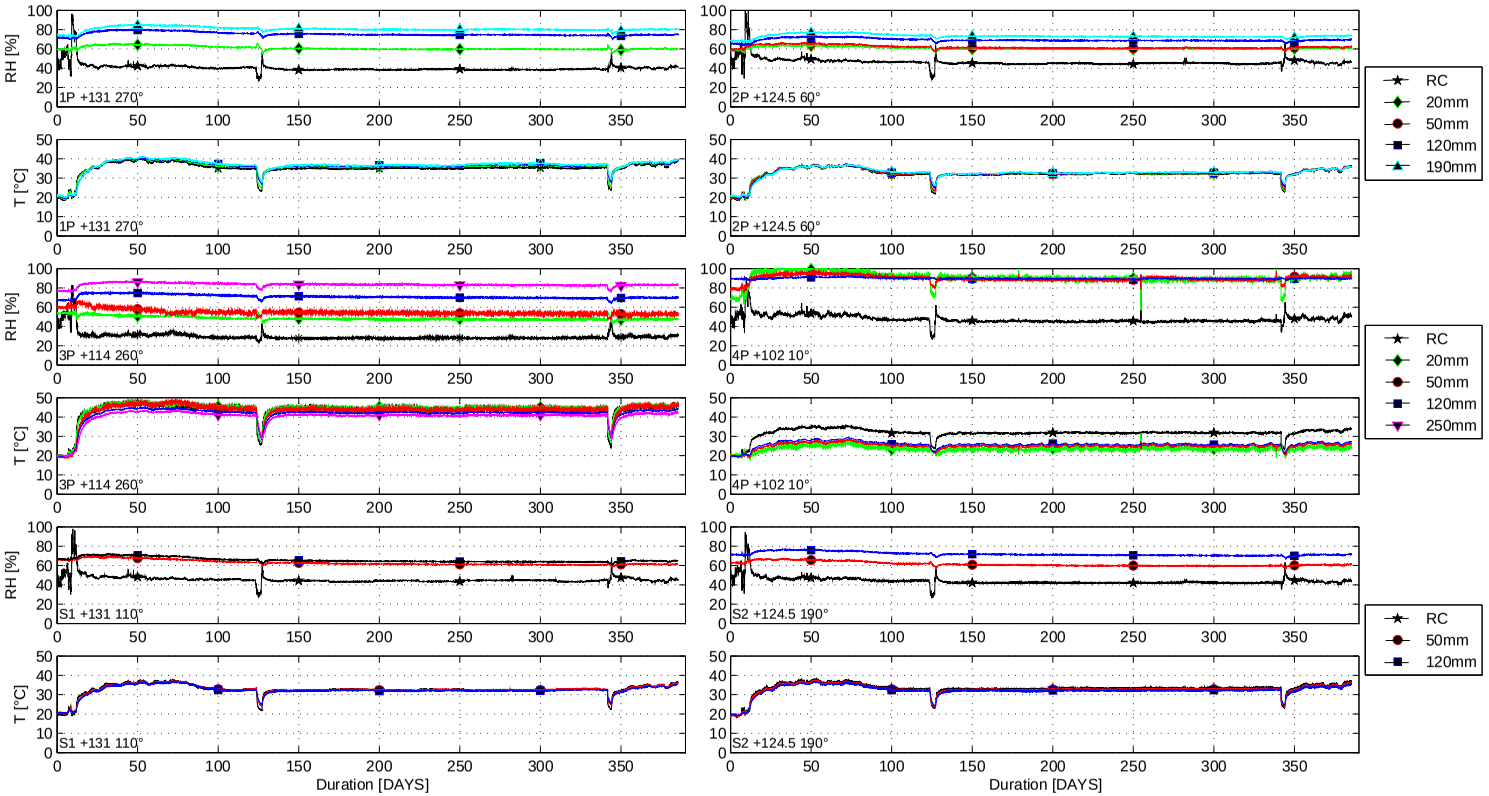

Figure 30. Measured results with adjustments, as described in **Paper V**, from the monitoring campaign in the RC at Forsmark 2. The measurements on Forsmark 2 started in June 2012 and were conducted until July 2013. Measurements were done in six zones in accordance with the details in Figure 29 and Table 10. Adjustments were done in zones 3P and 4P.

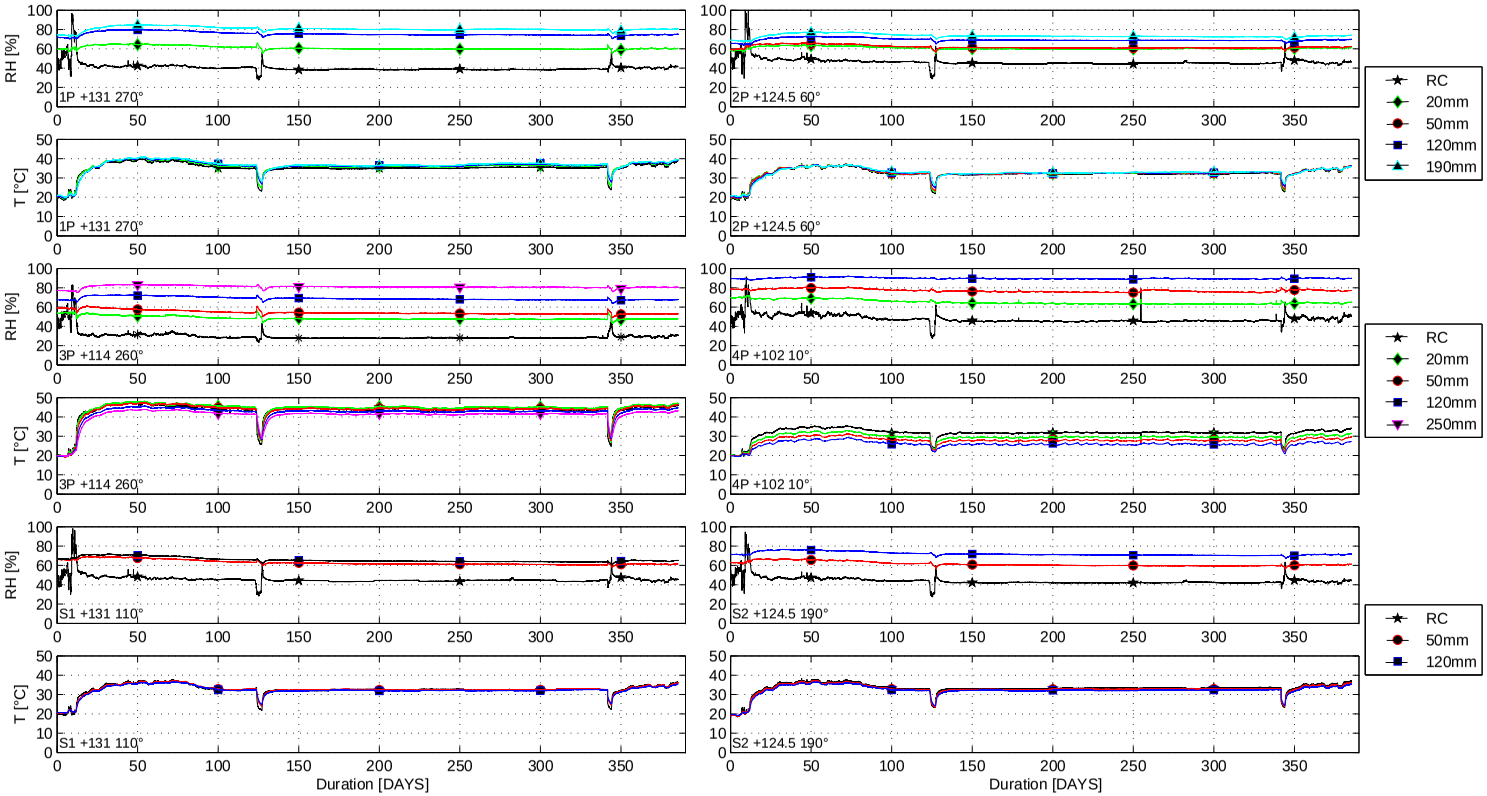

Figure 31 Measured results without adjustments, as described in **Paper V**, from the monitoring campaign in the RC at Forsmark 2. The measurements on Forsmark 2 started in June 2012 and were conducted until July 2013. Measurements were done in six zones in accordance with the details in Figure 29 and Table 10.

5.3 Measurements at Forsmark 3

In Table 11, the positions of the zones are presented, and Figure 32 shows a section of the containment where the position in terms of the height of the zones is illustrated. The measured results during one operational year is presented in Figures 33 and 34.

Table 11. Horizontal and vertical position of each zone at Forsmark 3, four primary (P) and two secondary (S) measurements. The steam pipes were located at 0° in the upper drywell and the personnel sluice at 90°. The +height 100 corresponds to sea level.

Zone	Depth [mm]	+ Heights [m]	Distance from centre [m]	Angle [°]
1P	Air: 30: 50: 150: 240	123	12.75	247
2P	Air: 30: 50: 120: 240	129	12.75	337
3P	Air: 30: 30: 50	114.5	6.10	250
4P	Air: 30: 30: 50	105.5	6.10	253
S1	Air: 50: 150	124.2	11.00	151
S2	Air: 50: 150	128	11.00	250

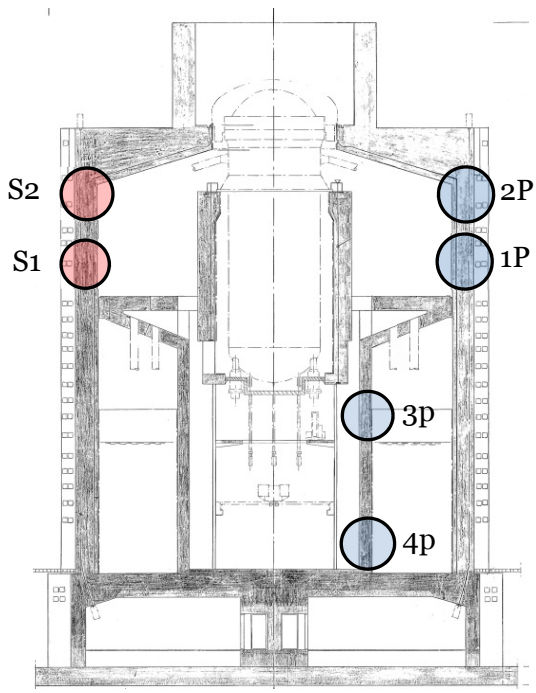

Figure 32. Section of Forsmark 3 with a schematic location of measurement zones. Zones 1P, 2P, S1, and S2 were located in the inner containment wall, and zones 3P and 4P in the wall separating the lower drywell and wetwell.

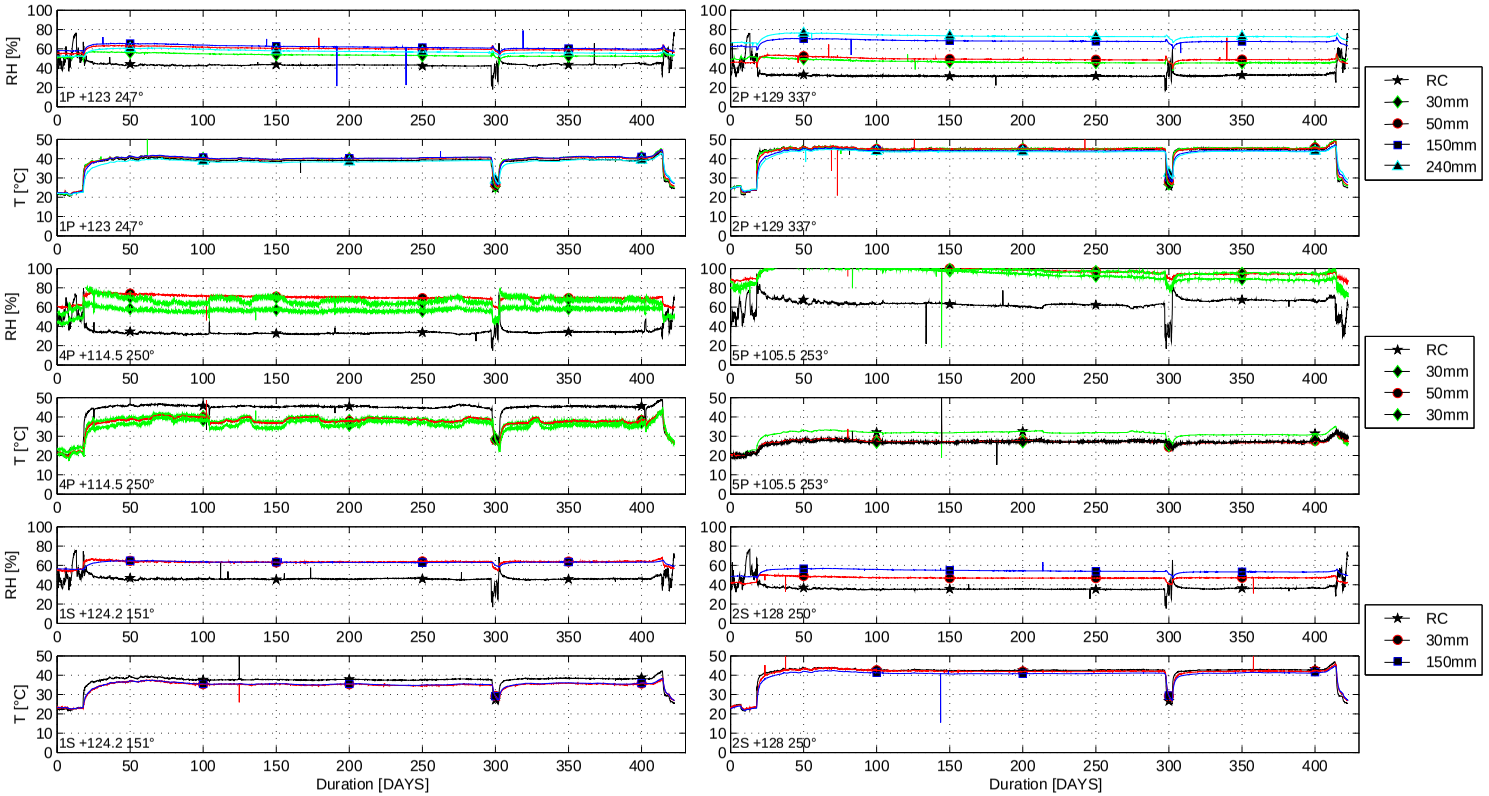

Figure 33 Measured results with adjustments, as described in **Paper V**, from the monitoring campaign in the RC at Forsmark 3. The measurements on Forsmark 3 started in July 2014 and were conducted until August 2014. Measurements were done in six zones in accordance with details in Figure 32 and Table 11. Adjustments were done in zones 4P, 5P, 1S, and 2S

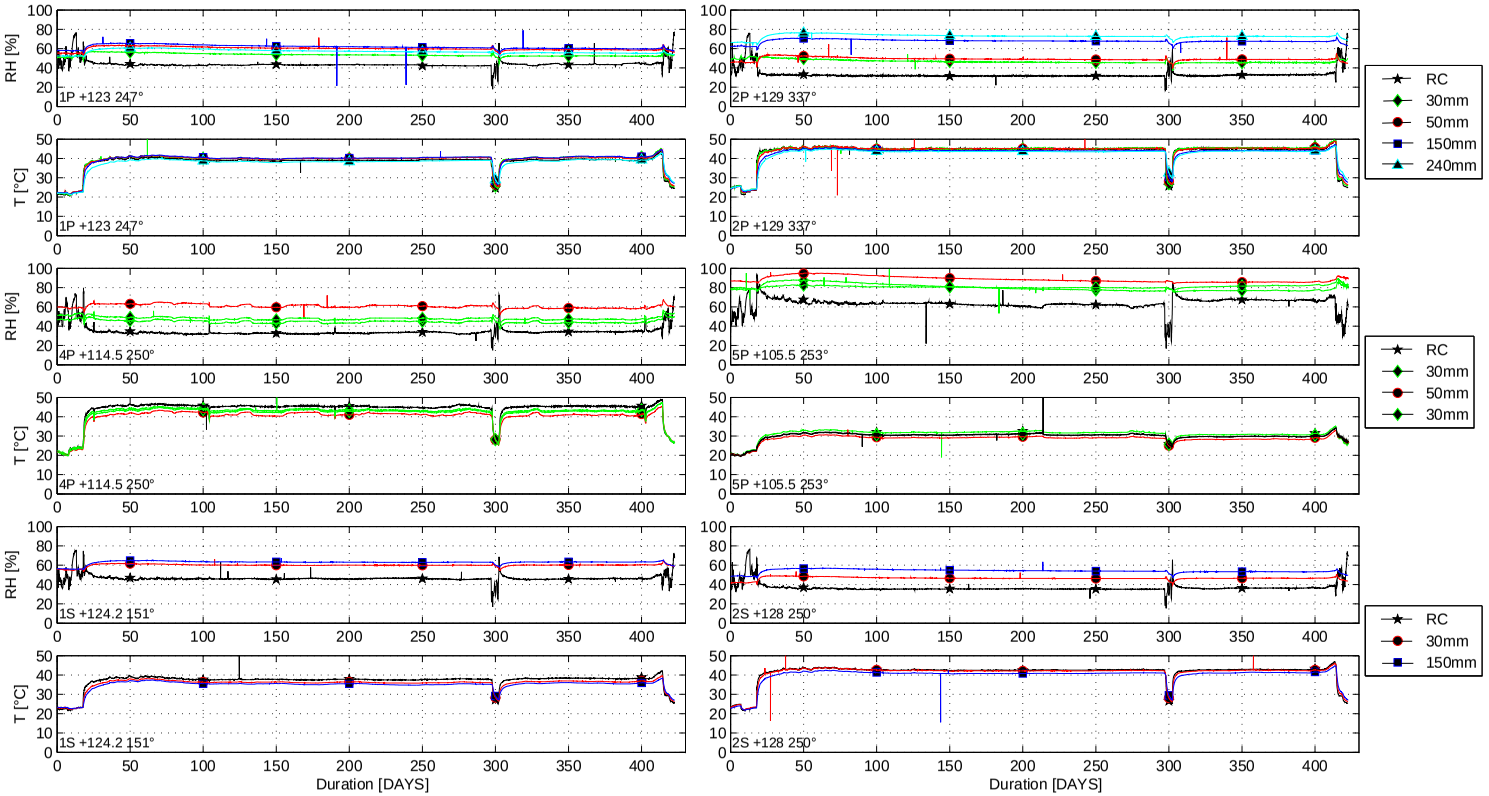

Figure 34. Measured results without adjustments, as described in **Paper V**, from the monitoring campaign in the RC at Forsmark 3. The measurements on Forsmark 3 started in July 2014 and were conducted until August 2014. Measurements were done in six zones in accordance with details in Figure 32 and Table 11.

5.4 Measurements at Ringhals 4

In Table 12, the positions of the zones are presented, and Figure 35 shows a section of the containment where the position in terms of the height of the zones is illustrated. The measured results during one operational year is presented in Figures 36 and 37.

Table. 12. Horizontal and vertical position of each zone at Ringhals 4, five primary (P) measurements. The personal sluice is located at 90° and the steam pipes exits at 270°.

Zone	Depth [mm]	+ Heights [m]	Distance from centre [m]	Angle [°]
1P	Air: 20: 50: 150: 240	134.5	17.50	90
2P	Air: 20: 50: 150: 240	115	17.50	130
3P	Air: 20: 50: 150: 240	95	17.50	140
4P	Air: 20: 50: 150	107	5.25	180
5P	Air: 20: 50: 150: 400	93	17.50	150

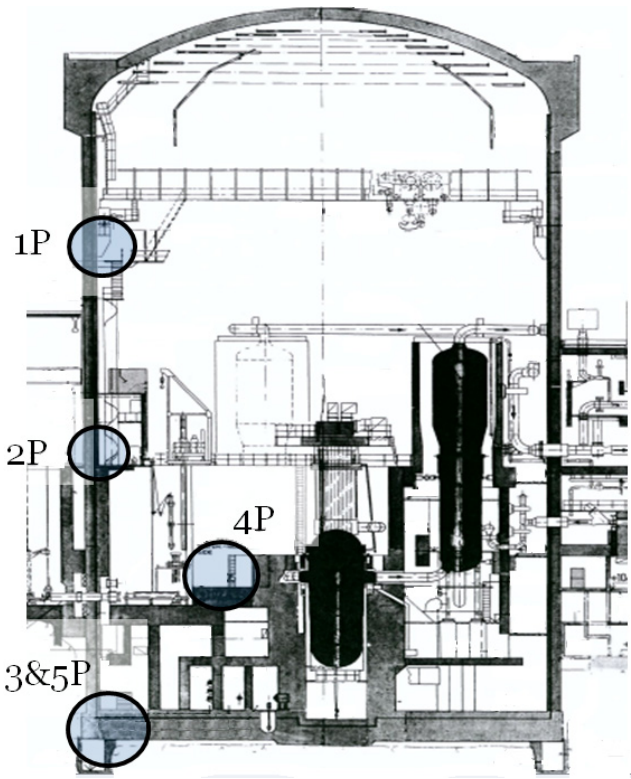

Figure 35. Section of Ringhals 4 with a schematic location of measurement zones. Zones 1P, 2P and 3P were located in the inner containment wall, zone 4P in the basin wall and zone 5P in the bottom slab.

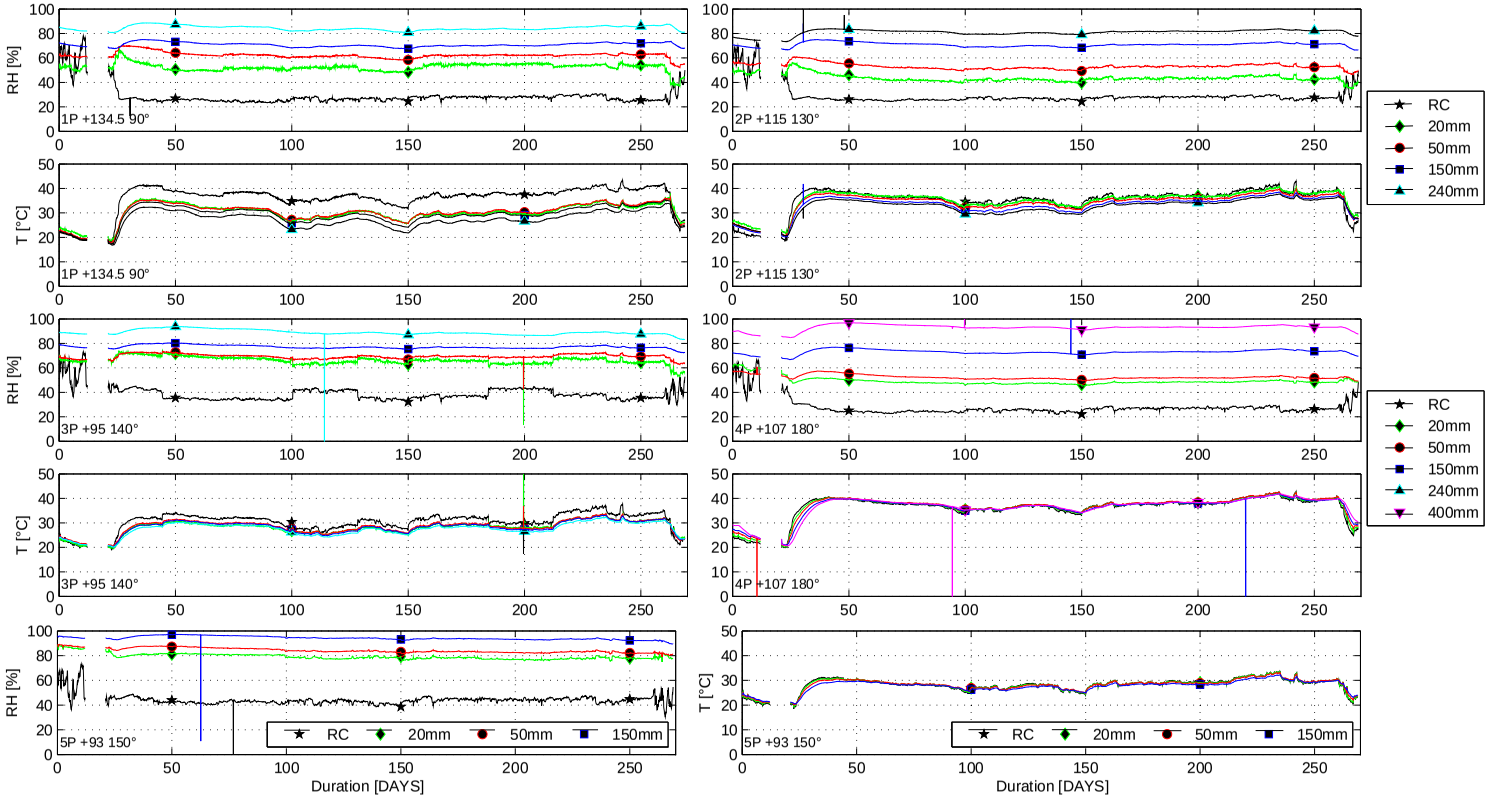

Figure 36. Measured results with adjustments, as described in **Paper V**, from the monitoring campaign in the RC at Ringhals 4. The measurements on Ringhals 4 started in August 2012 and were conducted until May 2013. Measurements were done in five zones in accordance with details in Figure 35 and Table 12. Adjustments were done in zones 1P, 2P, and 3P.

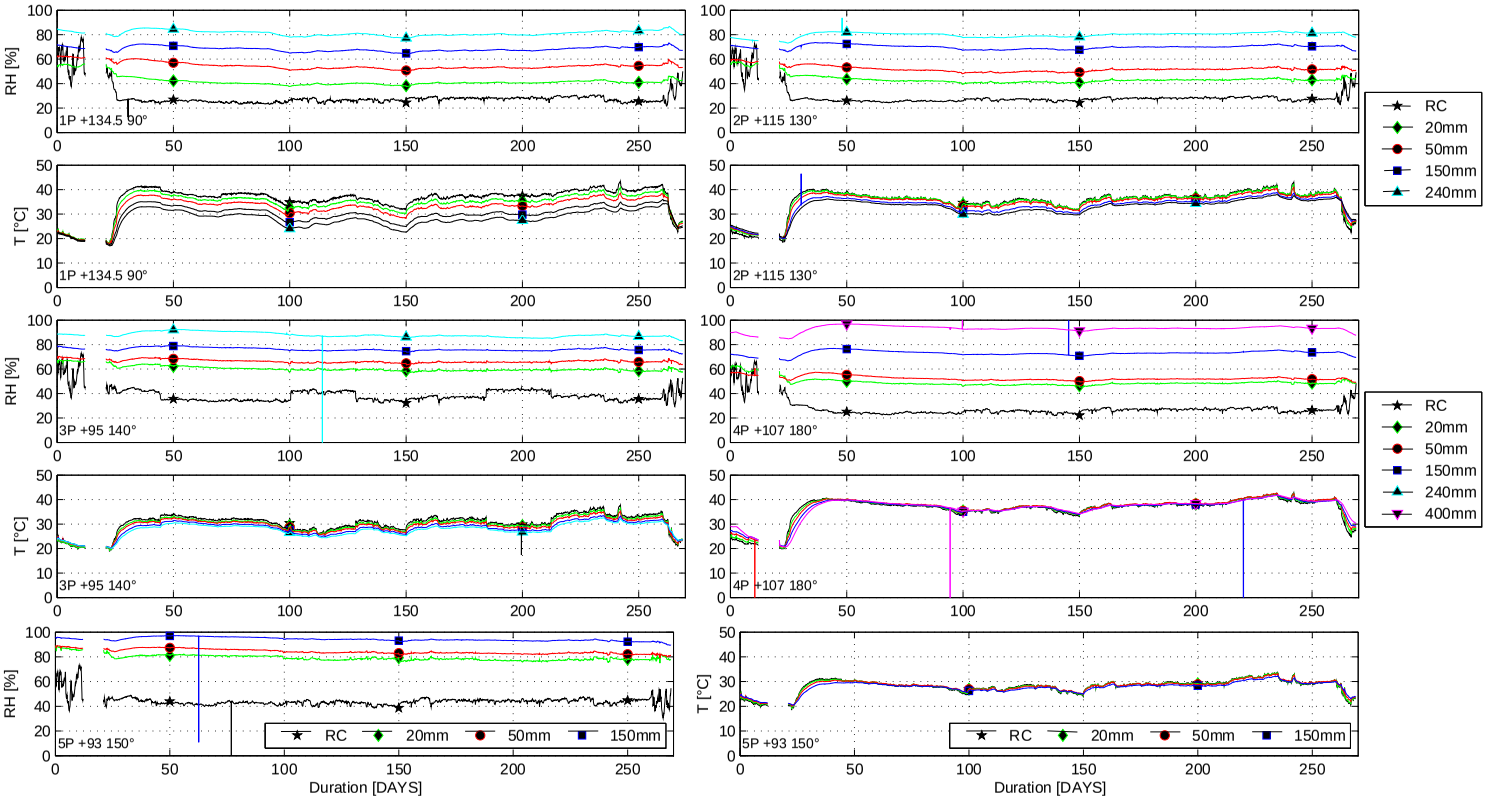

Figure 37. Measured results without adjustments, as described in **Paper V**, from the monitoring campaign in the RC at Ringhals 4. The measurements on Ringhals 4 started in August 2012 and were conducted until May 2013. Measurements were done in six zones in accordance with details in Figure 35 and Table 12.

6 Moisture contribution

A model was developed in this study to evaluate the ongoing moisture transport in different concrete components within the reactor containments during operation. The purpose of the model was to describe the ongoing processes as well as predict future conditions. The model is briefly presented in Chapter 4, and is given by Eq. 9. A thorough presentation of the model can be found in **Paper VI**. The model was validated by in situ measurements, as described in Chapter 5. The model was used to evaluate the conditions in the inner containment wall at the Nordic BWRs and predict its moisture contribution to the ambient compartments. The inner containment wall was chosen because it has similarities in different BWRs, and also covers all the regions of the upper drywell, allowing an evaluation of the whole compartment.

A MATLAB function for simulation of the ongoing drying of the reactor containments was designed using forward differential equations based on the model presented earlier. The structure of the function was designed as a main subroutine that communicated with the main loop. The main loop corresponds to one operational year. The operational year of the BWRs and the corresponding boundary conditions for the concrete components were divided into one outage period and one operational period. This was done based on the findings regarding seasonal changes, as presented in **Paper II**. Continuous changes in temperature and RH, as those observed at a PWR, require a more advanced non-isothermal model.

Simulations of the process for each year was further subdivided to cope with boundary variations, and the output from each subperiod was used as input in the following period. The same system applies for each year's cycle. A schematic illustration of the model design is shown in Figure 38. The material properties, sorption isotherms and moisture transfer coefficient were covered in additional subroutines, and used by the subcalculation loops. The subcalculation loop calculated the flux between each cell, and the new condition was calculated by the sum of the derivatives of the sorption isotherm.

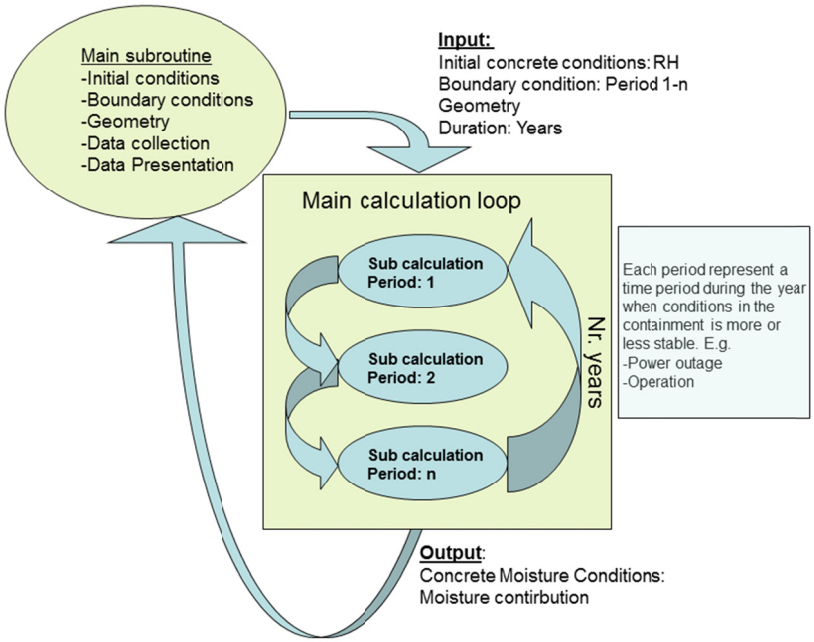

Figure 38. Schematic illustration of the model used for calculations. The function used subroutines which handle the material properties and moisture flux calculations.

The inputs needed for the model were the following: number of concrete volumes, total containment space, total time of exposure, time step, power outage period, operational period, initial concrete RH, thickness of the walls, wall area, outage boundary conditions and operational boundary conditions. The inputs used for the simulations of the BWRs are presented in **Appendix 1.**

A preliminary moisture contribution study, covered in **Paper IV,** presents rough calculations on the moisture transport at Ringhals 4 and Forsmark 2. The calculations were performed through non-isothermal moisture transport simulations, as given in Eq. 10 (*Section* 4.2), based on the average moisture conditions on the 95th day at Forsmark 2 and on the 100th day at Ringhals 4. A rough estimate of the moisture contribution showed that the concrete within the reactor containment cannot be neglected.

The results presented in **Paper VI** regarding moisture contribution from the inner containment walls at Nordic BWRs were in line with those in the preliminary study, as presented in **Paper IV**. The simulations additionally delivered predictions of future conditions as well as earlier moisture profiles and moisture flux. The results from the simulations of the three BWRs are presented in Figures 39–41. In Table 13, the results regarding total and yearly average moisture flux are presented. The drywell was divided into sections based on internal variations; however, no differences were observed for the Forsmark 2, and thus they were considered as one section.

Table 13. Predicted moisture contribution from the containment wall in the upper drywell at three BWRs. The table presents the average moisture flux during operation, accumulated flux, total moisture contribution for the entire containment wall and the theoretical remaining evaporable water still in the concrete based on the initial moisture content at full hydration. The values correspond to the following conditions: Forsmark 2: after 31 years, Forsmark 3: after 28 years, Ringhals 1: after 36 years, as well as after 60 years.

	Forsmark 2	Forsmark 3		Ringhals 1	
		Upper	Lower	Upper	Lower
Avg. Flux [g m^{-2} day^{-1}]	0.48	0.69	0.54	0.67	0.55
Avg. Flux, 60 Years [g m^{-2} day^{-1}]	0.25	0.24	0.23	0.31	0.45
Accum. Flux [kg m^{-2}]	8.52	11.38	8.69	17.82	8.03
Accum. Flux, 60 Years [kg m^{-2}]	11.83	15.80	12.63	20.20	10.17
Tot. H2O contr. [m^3]	5.5	7.2		12.3	
Tot. H2O contr.60 years [m^3]	7.7	10.2		14.4	
Evaporable water	65 %	61 %		54 %	
Evaporable water, 60 Years	53 %	44 %		46 %	

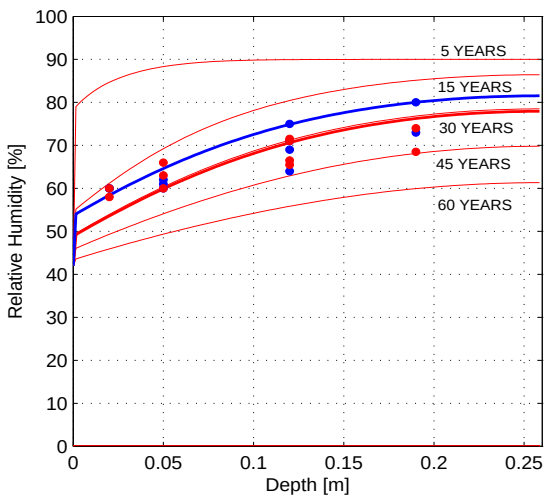

Figure 39. Results from simulations of Forsmark 2, giving the RH distribution within the containment wall after 5, 15, 30, 45 and 60 years. The symbols represent the measured conditions after 31 years of operation, during the power outage (red) and during operation (blue). The thick lines are the simulated RH distribution after 31 years, both during operation (blue) and during power outage (red).

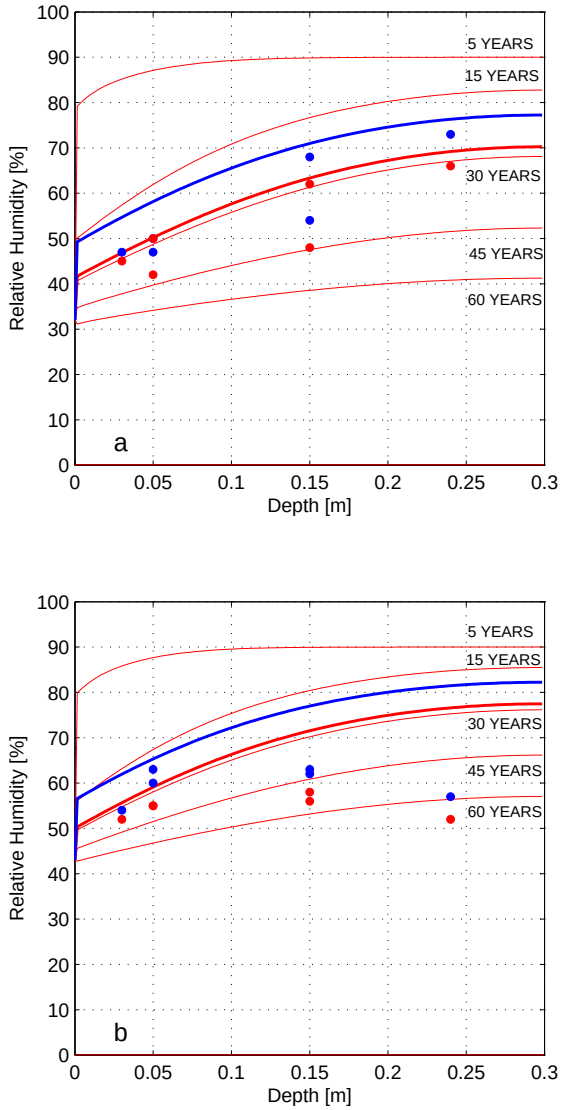

Figure 40. Results from simulations of Forsmark 3 giving the RH distribution within the containment wall after 5, 15, 30, 45 and 60 years, where **a** and **b** correspond to the upper and lower parts, respectively. The symbols in the figure represent the measured conditions after 28 years of operation, during power outage (red) and during operation (blue). The thick lines are the simulated RH distribution after 28 years, both during operation (blue) and during power outage (red).

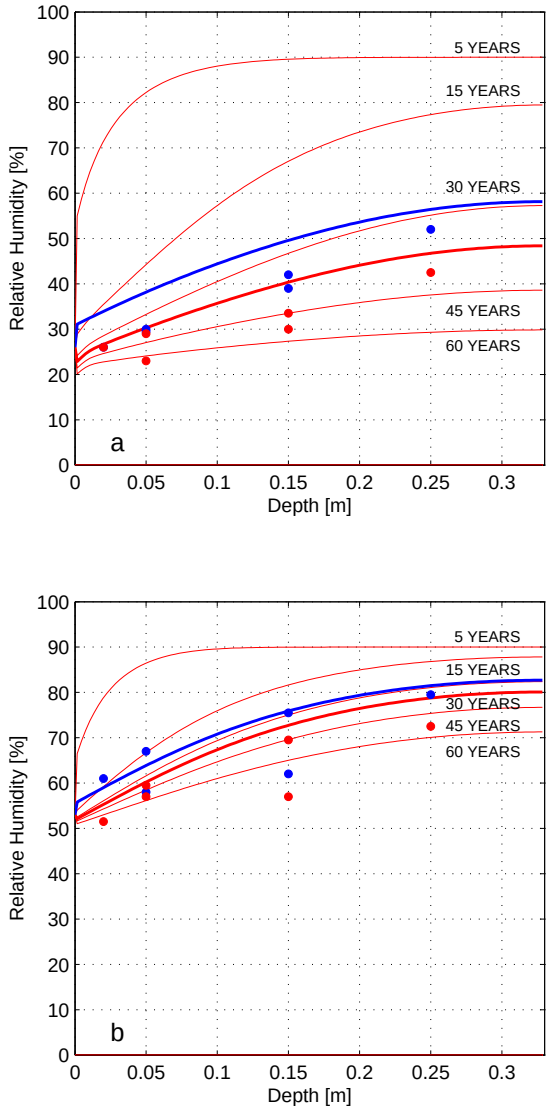

Figure 41. Results from simulations of Ringhals 1 giving the RH distribution within the containment wall after 5, 15, 30, 45 and 60 years, where **a** and **b** correspond to the upper and lower parts, respectively. The symbols in the figure represent the measured conditions after 36 years of operation, during power outage (red) and during operation (blue). The thick lines are the simulated RH distribution after 36 years, both during operation (blue) and during power outage (red).

7 Concluding remarks

The moisture contributions from the concrete as well as from other moisture sources have to be known to reliably evaluate the moisture condition within a reactor containment. Systematic measurements of the moisture conditions of interior air and concrete are needed to understand to some extent, the prevailing moisture condition in a reactor containment and the expected contribution from the concrete structures in contact with the interior air. By measuring the moisture profiles in the concrete structures during operation and the boundary conditions at the concrete surfaces, the actual moisture conditions in the structures and the drying rate could be determined. These data were thereafter used to validate a model to determine the past and future moisture conditions in the concrete structures in the rector containment.

A measurement setup was designed and evaluated in this project. The setup was used in the monitoring campaigns at four NPPs in Sweden in order to describe the conditions within the different containments during an operational year. The monitoring campaigns were designed to describe the overall conditions, both in the compartments and in the concrete structures. Equivalent zones and concrete structures were chosen at the NPPs to evaluate internal variations as well as similarities and differences between the different NPPs. The inner containment wall was chosen as the main structure for the comparisons, as the design was similar between all NPPs included in this study, and because of its being one of the larger structures in each containment.

A stable and reliable measurement setup was essential to ensure that the conditions monitored can be considered as accurate. Because of this requirement, the setup was thoroughly tested in evaluations in controlled conditions, as given in **Papers IV and V**, through computer simulations, as given in **Paper V**, and in situ measurements, as given in **Papers III and IV**. It was concluded from these evaluations that the setup was stable and valid for long term monitoring in concrete structures when in isothermal condition. Based on the results, it was concluded that measurements at shallow depths, i.e. 20 and 50 mm, have to be treated with more attention. Later results from the moisture transport model, as presented in **Paper VI**, however showed that in some zone, e.g. zone 1P at Ringhals 1, the concrete was exposed for drying and rewetting, and consequently, what was earlier suggested as leakage is most likely the moisture movement. It was concluded that measurements at shallow depths require more attention and that a revision of the opening gap sealant system is needed.

The largest error while using the test setup was found when temperature differences between the concrete and the surroundings occurred. Because of the design of the setup, the

temperature measurements in the concrete were directly affected by the ambient temperature and required a correction in this misread value. An evaluation in a laboratory condition, presented in **Paper V**, showed that the effect was large while measuring at shallow depths, and this effect had to be considered. This effect reduced with depth, and for measurements at depths greater than 100 mm, the temperature misread directly correlated to the temperature gradient in the material, and not to the ambient conditions. However, from the evaluations, it was not possible to deliver a universal tool to cope with these errors, as site specific conditions affect the influence, e.g. through variation of surface thermal resistance. Based on the findings, it is suggested that the surface temperature is to be measured in order to better adjust the measurements when in non-isothermal conditions.

The measurements in situ presented in this thesis, together with the information in **Papers I, II, III, IV** and **VI**, represent the first instance when such monitoring inside NPPs have been done systematically and published. The measurements show that there are several similarities while comparing the different NPPs with regard to the climatic conditions within different compartments, as well as the conditions within the concretes structures. Furthermore, the measurements show that there are large variations between all containments included in this study, both while comparing NPPs of the same type and of different types. In view of these findings, similar measurements are required at other NPPs for a proper evaluation of their specific conditions. The results presented here should, however, be considered as an approximation of the conditions expected for the other NPPs.

The differences observed between the NPPs are a result of differences in the designs of the inner structures, variations in the internal climatic conditions and the effect of outdoor temperature, as presented in **Paper II**. Even though some of the NPPs have several design similarities, climatic differences are observed. One clear example is while comparing Forsmark 2 and Forsmark 3, where the measurements show clear internal variations in the upper drywell at Forsmark 3, but almost no variation at Forsmark 2. The large variations between the NPPs are considered to be due to the absence of regulation regarding humidity levels within the RC and concrete, as well as due to a wide array of design regulations regarding acceptable concrete temperatures. Based on the measurements it was concluded that all NPPs were within the regulated temperature intervals, even though large variations occurred. It was also concluded, based on the stable conditions within the containments, that the humidity within the containments are "as-designed". The constant humidity was most likely due to the continuous dehumidification; however, in this project, it was not possible to determine the exact quantity of dehumidified water during the year of operation.

A moisture transport model was developed to address the variations in the conditions within the Nordic BWRs, presented in **Paper VI**. Only the BWRs were evaluated because of a more complex condition existing within the PWRs. Based on the study presented in **Paper II,** it was concluded that because of the rapid temperature variations in concrete structures, as well as in the ambient air, a more advanced non-isothermal model was needed for the PWR. It was further concluded that it is not possible to derive a non-isothermal model in this study because of the absence of the relevant material properties, and methods to determine them.

Simulations of moisture transport within the inner containment wall in the upper drywell at the BWRs was done through a new MATLAB function that was based on the new model and simulated through forward differential equation loops. The model was validated by comparing the simulations with the in situ measurements, as presented in Chapter 5 and **Paper VI,** using the equipment and setup designed and evaluated in **Papers III, IV** and **V**. The simulations showed reasonable correlation and acceptable agreement with the measured conditions. The model was thus considered to deliver a fairly good approximation of the future conditions as well as describe the earlier conditions with acceptable accuracy. Complementary measurements are however needed within 5–15 years to validate the continuing drying equivalent to that predicted by the simulations. The largest source of error in the simulations is considered to be inaccurate material properties and the conditions before the reactors were put into operation.

The results of the moisture transport simulation and measurements led to the conclusion that the concrete components within the containments were still drying and emitted vapour to the interior air. The simulated results of approximately 30 years of operation indicated drying of 35–45 % of the initial evaporable water. If similar exposure is considered until 60 years of operation, this would result in a total drying of 45–55 % of the initial evaporable water. The main drying of the structures has thus already occurred, and the moisture contribution to the ambient compartments will continue to decrease further.

As it was not possible to quantify the total quantity of water that was collected by the dehumidification equipment, the actual contribution could not be evaluated. It was therefore not possible to determine whether the drying of concrete was the main source of moisture or whether it was negligible. It was however concluded that the concrete within the containments did contribute with a considerable amount of water. As an example, 10 % of the concrete at Forsmark 2 has contributed with five cubic meters of water as the reactor was put into operation until the time of monitoring. The total contribution from Forsmark 3 and Ringhals 1 was seven and twelve cubic meters of water, respectively, as they were started until the monitoring campaigns were conducted.

The consequence of drying of the concrete within the containments are not obvious. Different moisture levels in concrete have advantages as well as negative aspects. A high RH in the concrete may result in an increased risk of corrosion of the metal within the concrete, provided that an air cavity exists between the concrete and the metal surface. A high RH, however, drastically reduces the CO_2 ingress, and hence the carbonation, and consequently reduces corrosion of the reinforcement. Moreover, a high RH is essential for the hydration of the cement. The moisture content within the concrete is also a key element for the radiation shielding properties, which reduce drastically with a decreasing moisture content. A large moisture contribution to the surroundings may lead to surface condensation on metal surfaces on ambient structures and consequently pose an increased risk of surface corrosion. Drying of concrete also leads to increase in shrinkage and creep.

The optimal moisture conditions in concrete differ for different structures within the containments. In the case of a new build, the concrete structures could be designed based

on the main function of the specific structures; this might however not be possible or be expensive. The second best approach is to have the knowledge of the moisture conditions that can be expected in the different structures. In the case of a new build, the concrete used as well as the structures should be properly evaluated. Further, the specific material parameters needed to predict the future conditions should be determined, and concrete samples should be stored for future analyses.

8 Future Research

With regards to the results presented in this doctoral thesis, the following are suggested as future research issues.

- Further research is needed in order to increase the accuracy of the RH measurements in non-isothermal conditions. Without accurate measurements, it is difficult to develop and verify accurate moisture transport models as well as to describe the actual conditions in a structure. The set-up developed in this work failed to reach the same level of accuracy in the non-isothermal conditions as in the isothermal conditions.

- A model was suggested in this study to describe the conditions within different reactor containment, and how the conditions vary with time. The model was however not sufficient in order to describe all the conditions relevant for any type of nuclear reactor containment. The model was developed only to describe a quasi-uniform moisture transport model and was not applicable for the entirely non-isothermal conditions, such as those observed in the containment wall at a Nordic PWR. A non-isothermal moisture transport model should be designed to describe the moisture transport processes within a nuclear reactor containment. The model should include properties such as the moisture fixation hysteresis as well as the moisture and temperature dependency of the material.

- The obtained results from this thesis gives great potential for further evaluation and research of the effects from the moisture conditions within different concrete structures located in the containment. Multiple material parameters and conditions are moisture dependent, such as creep and shrinkage, gas tightness and radiation shielding properties. The same compiles for several degrading mechanisms such as corrosion and carbonation. Further research is needed within these fields in order to increase the awareness of the conditions of the reactor containments.

- Further work is needed in order to compare the obtained results of the moisture contribution from the concrete structures. The actual impact of the concrete drying within the containment has not yet been quantified.

- Follow-up in situ measurements within 5-10 years is further suggested in order to validate the accuracy of the model and simulations of future predictions presented in this thesis.

Reference

1. J. Picaut, et al., *Nuclear containments*, in *fib State-of-art report*. 2001, International Federation for Structural Concrete (fib): Lausanne, Switzerland.
2. C.P. Thorne, *Concrete properties relevant to rector shield behaviour.* Journal of the American concrete institute, 1961. **32**(11): p. 1491-1508.
3. L. Barcelo, M. Moranville, and B. Clavaud, *Autogenous shrinkage of concrete: a balance between autogenous swelling and self-desiccation.* Cement and Concrete Research, 2005. **35**(1): p. 177-183.
4. P. Fredlund and L.-O. Nilsson, *Gas penetration in concrete reactor containments - Measurements and Modelling (In Swedish)*, in *Elforsk rapport 09:101*. 2009, Lund University, Division of Building Materials: Lund, Sweden.
5. H.K. Hilsdorf, *A method to estimate the water content of concrete shields.* Nuclear Engineering and Design, 1967. **6**(3): p. 251-263.
6. M. Åhs, *Redistribution of moisture and ions in cement based materials,* Doctoral Thesis. 2011. Lund University, Lund, Sweden
7. L.-O. Nilsson, *Hygroscopic moisture in concrete - drying, measurements & related material properties,* Doctoral Thesis. 1980. Lund University, Lund, Sweden
8. H.-W. Song, et al., *Creep prediction of concrete for reactor containment structures.* Nuclear Engineering and Design, 2002. **217**(3): p. 225-236.
9. Z. Grasley, D. Lange, and M. D'Ambrosia, *Internal relative humidity and drying stress gradients in concrete.* Materials and Structures, 2006. **39**(9): p. 901-909.
10. Z. Grasley and D. Lange, *Thermal dilation and internal relative humidity of hardened cement paste.* Materials and Structures, 2007. **40**(3): p. 311-317.
11. Z.P. Bažant, *Delayed thermal dilatations of cement paste and concrete due to mass transport.* Nuclear Engineering and Design, 1970. **14**(2): p. 308-318.
12. Z. Hora and B. Patzák, *Analysis of long-term behaviour of nuclear reactor containment.* Nuclear Engineering and Design, 2007. **237**(3): p. 253-259.
13. H. Kagimoto and M. Kawamura, *Measurements of strain and humidity within massive concrete cylinders related to the formation of ASR surface cracks.* Cement and Concrete Research, 2011. **41**(8): p. 808-816.
14. G. Fagerlund, *Critical degree of saturation at freezing of porous and brittle materials,* Doctoral Thesis. 1972. Lund University, Lund, Sweden

15. K. Fridh, *Internal frost damage in concrete- Experimental studies of destruction mechanisms,* Doctoral Thesis. 2005. Lund University, Lund, Sweden
16. D.-W. Ryu, J.-W. Ko, and T. Noguchi, *Effects of simulated environmental conditions on the internal relative humidity and relative moisture content distribution of exposed concrete.* Cement and Concrete Composites, 2011. **33**(1): p. 142-153.
17. C. Andrade, J. Sarrıa, and C. Alonso, *Relative humidity in the interior of concrete exposed to natural and artificial weathering.* Cement and Concrete Research, 1999. **29**(8): p. 1249-1259.
18. L.-O. Nilsson, *Drying of reactor containment walls of concrete during past and future decades*, in *SMiRT 19*. 2007, International association of structural mechanics in reactor technology: Toronto.
19. A. Courtois, et al., *Water Content Monitoring for Nuclear Concrete Buildings: Needs, Feedback and Perspectives.* Poromechanics, 2013. **V**: p. 1654-1663.
20. P. Johansson and L.-O. Nilsson, *Climatic conditions at the surfaces of concrete containments - examples for two BWR and PWR reactors*, in *SMiRT 19*. 2007: Toronto.
21. L.-O. Nilsson and P. Johansson, *Changes in reactor containments - The drying and climatic conditions in the concrete walls (In Swedish)*, in *Elforsk rapport 09:100*. 2009, Lund University, Division of Building Materials: Lund, Sweden.
22. M. Åhs, et al., *A model to predict moisture conditions in concrete reactor containments*, in *Fontevraud 8, Contribution of materials investigations and operating experience to LWRs' safety, performance and reliability*. 2014: Avignon.
23. IAEA, *Assessment and management of ageing of major nuclear power plant components important to safety: Concrete containment building*, in *IAEA-TECDOC Series*. 1998, IAEA: Vienna, Austria.
24. IAEA, *Defence in depth in nuclear safety: INSAG-10* in *INSAG series*. 1996, IAEA: Vienna, Austria.
25. IAEA, *Design of reactor containment systems for nuclear power plants*, in *Safety standards series*. 2004, IAEA: Vienna, Austria.
26. I. Akkurt, et al., *Gamma-ray shielding properties of concrete including barite at different energies.* Progress in Nuclear Energy, 2010. **52**: p. 620-623.
27. S. Alhajali, et al., *Estimation of the activation of local reactor shielding concretes.* Progress in Nuclear Energy, 2009. **51**(2): p. 374-377.
28. L. Chang-Min, L. Yoon Hee, and L. Kun Jai, *Cracking effect on gamma-ray shielding performance in concrete structure.* Progress in Nuclear Energy, 2007. **49**: p. 303-312.
29. M.H. Kharita, M. AlNassar, and S. Yousef, *The effect of the initial water to cement ratio on shielding properties of ordinary concrete.* Progress in Nuclear Energy, 2010. **52**(5): p. 491-493.

30. M.H. Kharita, et al., *Development of special radiation shielding concretes using natural local materials and evaluation of their shielding characteristics.* Progress in Nuclear Energy, 2008. **50**(1): p. 33-36.
31. M.H. Kharita, S. Yousef, and M. AlNassar, *Review on the addition of boron compounds to radiation shielding concrete.* Progress in Nuclear Energy, 2011. **53**(2): p. 207-211.
32. T. Korkut, et al., *A new radiation shielding material: Amethyst ore.* Annals of Nuclear Energy, 2011. **38**(1): p. 56-59.
33. F. Vodák, et al., *Effect of gamma irradiation on properties of hardened cement paste.* Materials and Structures/Materiaux et Constructions, 2011. **44**(1): p. 101-107.
34. IAEA, *Operating experience with nuclear power stations in member states in 2011*. 2012, IAEA: Vienna, Austria.
35. T. Roth, J. Silfwerbrand, and H. Sundqvist, *Concrete reactor containments at Swedish Nuclear Power Plants (In Swedish)*. 2002, KTH Royal Institute of Technology: Stockholm, Sweden.
36. ACI, *Code Requirements for Nuclear Safety Related Concrete Structures*, in *(ACI 349-01)*. 2001, American Concrete Institute.
37. ACI-ASME, *Code for Concrete Reactor Vessels and Containments*, in *ACI 359-01*. 2001, American Society of Mechanical Engineers. p. 437-457.
38. L.-O. Nilsson and P. Johansson, *The moisture conditions of nuclear reactor concrete containment walls – an example for a BWR reactor.* J. Phys. IV France, 2006. **136**: p. 141-150.
39. L.-O. Nilsson. *Moisture transport under temperature gradient - Some old and new studies*. in *Understanding the fundamental properties of concrete. Celebrating Prof. Erik J. Sellevold on his 75th birthday*. 2013. Trondheim.
40. E. Drouet, S. Poyet, and J.-M. Torrenti, *Temperature influence on water transport in hardened cement pastes.* Cement and Concrete Research, 2015. **76**: p. 37-50.
41. S. Whitaker, *Simultaneous Heat, Mass, and Momentum Transfer in Porous Media: A Theory of Drying*. 1977, Elsevier. p. 119-203.
42. M. Jensen, B. Johannesson, and M. Geiker, *A Numerical Comparison of Ionic Multi-Species Diffusion with and without Sorption Hysteresis for Cement-Based Materials.* Transport in Porous Media, 2015. **107**(1): p. 27-47.
43. J.R. Philip and D.A. De Vries, *Moisture movement in porous materials under temperature gradients.* American Geophysical Union, 1957. **38**(2): p. 222-232.
44. A.V. Luikov, *Heat and Mass Transfer in Capillary-Porous Bodies*, in *Advances in Heat Transfer*, F.I. Thomas and P.H. James, Editors. 1964, Elsevier. p. 123-184.
45. H.P. Lien and F.H. Wittmann, *Mass transfer in inhomogeneous porous media under thermal gradients.* Nuclear Engineering and Design, 1998. **179**(2): p. 179-189.

46. H. Garbalińska, S.J. Kowalski, and M. Staszak, *Moisture Transfer Between Unsaturated Cement Mortar and Ambient Air.* Transport in Porous Media, 2010. **85**(1): p. 79-96.
47. D.A. De Vries, *The theory of heat and moisture transfer in porous media revisited.* International Journal of Heat and Mass Transfer, 1987. **30**(7): p. 1343-1350.
48. M. Janz, *Moisture transport and fixation in porous materials at high moisture levels,* Doctoral Thesis. 2000. Lund University, Lund, Sweden
49. J. Claesson, *A few remarks on moisture flow potentials*, in *TVBH-7163*. 1993, Lund University, Division of Building Physics: Lund, Sweden.
50. Z. Bažant and L. Najjar, *Nonlinear water diffusion in nonsaturated concrete.* Materials and Structures, 1972. **5**(1): p. 3-20.
51. Z.P. Bažant, *Thermodynamic theory of concrete deformation at variable temperature and humidity*. 1969, University of California: Berkeley.
52. G. Hedenblad, *Moisture permeability of mature concrete, cement mortar and cement paste,* Doctoral Thesis. 1993. Lund University, Lund, Sweden
53. M. Saeidpour and L. Wadsö, *Moisture diffusion coefficients of mortars in absorption and desorption.* Cement and Concrete Research, 2016. **83**: p. 179-187.
54. L. Greenspan, *Humidity Fixed Points of Binary Saturated Aqueous Solutions.* Journal of Research of the National Bureau of Standards. Section A: Physics and Chemistry 1977. **81A** (1): p. 89-96.
55. M. Hjorslev Hansen, *Estimation of transfer coefficients in models for coupled heat and moisture transfer in porous media,* Doctoral Thesis. 1993. Technical University of Denmark, Lyngby
56. A. Anderberg and L. Wadsö, *Method for simultaneous determination of sorption isotherms and diffusivity of cement-based materials.* Cement and Concrete Research, 2008. **38**(1): p. 89-94.
57. J.P. Ollivier, J.C. Maso, and B. Bourdette, *Interfacial transition zone in concrete.* Advanced Cement Based Materials, 1995. **2**(1): p. 30-38.
58. T.C. Powers and T.L. Brownyard, *Studies of the physical properties of hardened portland cement paste. Part 9. General summary of findings on the properties of hardened portland cement paste.* Journal of the American concrete institute, 1947. **18**(8): p. 971-992.
59. T. Hansen, *Physical structure of hardened cement paste. A classical approach.* Materials and Structures, 1986. **19**(6): p. 423-436.
60. H.F.W. Taylor, *Cement chemistry*. 2nd edition ed. 1997, London: Thomas Telford Publishing.
61. J.I. Bhatty and K.J. Reid, *Use of thermal analysis in the hydration studies of a type 1 portland cement produced from mineral tailings.* Thermochimica Acta, 1985. **91**(C): p. 95-105.
62. H.G. Midgley, *The determination of calcium hydroxide in set Portland cements.* Cement and Concrete Research, 1979. **9**(1): p. 77-82.
63. H.S. Wong and N.R. Buenfeld, *Determining the water-cement ratio, cement content, water content and degree of hydration of hardened cement paste: Method development and validation on paste samples.* Cement and Concrete Research, 2009. **39**(10): p. 957-965.

64. B. El-Jazairi and J.M. Illston, *A simultaneous semi-isothermal method of thermogravimetry and derivative thermogravimetry, and its application to cement pastes.* Cement and Concrete Research, 1977. **7**(3): p. 247-257.
65. I. Pane and W. Hansen, *Investigation of blended cement hydration by isothermal calorimetry and thermal analysis.* Cement and Concrete Research, 2005. **35**(6): p. 1155-1164.
66. L. Alarcon-Ruiz, et al., *The use of thermal analysis in assessing the effect of temperature on a cement paste.* Cement and Concrete Research, 2005. **35**(3): p. 609-613.
67. B.A. Schrefler, et al., *Thermo-hydro-mechanical modelling of high performance concrete at high temperatures.* Engineering Computations (Swansea, Wales), 2002. **19**(7-8): p. 787-819.

Appendix 1

Table 4. Input used for the simulations of the moisture transport in the containment walls at three Nordic BWRs using the model adapted for their conditions, as presented in **Paper VI** and Chapter 6.

	Forsmark 2	Forsmark 3		Ringhals 1	
		Upper	Lower	Upper	Lower
Tot, Duration [Years]	60	60	60	60	60
Time steps [hours]	3	3	3	3	3
Outage / Operation [month]	1 / 11	1 / 11	1 / 11	1 / 11	1 / 11
Wall thickness [mm]	260	300	300	330	330
Wall area [m2]	650	360	360	475	475
RH/T - Outage	50 %RH/20°C	40%RH/23.5°C	45%RH/22°C	45%RH/21.5°C	45%RH/21°C
RH/T - Operation	42 %RH/33°C	32%RH/45°C	43%RH/39°C	26 %RH/48°C	53%RH/31°C
Epoxy coating (Z_φ) [m^2 s kg^{-1}]	$21.6 \cdot 10^6$	$21.6 \cdot 10^6$	$21.6 \cdot 10^6$	$7.2 \cdot 10^6$	$7.2 \cdot 10^6$
Conc. δ_v < 65%RH [m^2 s^{-1}]	$0.56 \cdot 10^{-7}$	$0.56 \cdot 10^{-7}$	$0.56 \cdot 10^{-7}$	$0.56 \cdot 10^{-7}$	$0.56 \cdot 10^{-7}$
Moist.Cont 100 %RH [kg m^{-3}]	118	105	105	105	105
Moist.Cont 90 %RH [kg m^{-3}]	94	85	85	85	85